Calculation of parity-nonconserving effects in the $6^2P_{1/2}$-$7^2P_{1/2}$ forbidden $M1$ transition in thallium*

David V. Neuffer and Eugene D. Commins
Physics Department, University of California, Berkeley, California 94720
and Materials and Molecular Research Division, Lawrence Berkeley Laboratory, Berkeley, California 94720
(Received 4 April 1977)

Calculations are presented of the $E1$ amplitude expected in the $6^2P_{1/2}$-$7^2P_{1/2}$ forbidden $M1$ transition in Tl if parity conservation is violated in the neutral weak e-N interaction, as proposed in a number of gauge models, including that of Weinberg and Salam. Valence-electron wave functions are generated as numerical solutions to the Dirac equation in a modified Tietz central potential. These wave functions are used to calculate allowed $E1$ oscillator strengths, hfs splittings, and Stark $E1$ transition amplitudes. These results are compared with experiment and the agreement is generally good. The relativistic $6^2P_{1/2}$-$7^2P_{1/2}$ $M1$ transition amplitude $\mathfrak{M}$ is also calculated, and corrections due to interconfiguration mixing, Breit interaction, and hfs mixing are included. The result, $\mathfrak{M}_{\text{theor}} = (-3.2 \pm 1.0) \times 10^{-5} |e|\hbar/2m_ec$, is in agreement with the experimental value, $\mathfrak{M}_{\text{expt}} = (-2.11 \pm 0.30) \times 10^{-5} |e|\hbar/2m_ec$. The parity-nonconserving $E1$ amplitude $\mathcal{E}_{\text{PN}}$ is calculated, and a value for the circular dichroism, $\delta \simeq 2\text{Im}(\mathcal{E}_{\text{PN,theo}})/\mathfrak{M}_{\text{expt}} = 2.6 \times 10^{-3}$, is obtained. Parity-nonconserving effects in other Tl transitions are discussed.

I. INTRODUCTION

Discovery of strangeness-conserving neutral weak currents in neutrino-nucleon scattering experiments[1] has stimulated considerable interest in the possible existence of a weak neutral electron-nucleon interaction. If such an interaction violates parity conservation, as predicted by several theoretical gauge models including that of Weinberg and Salam[2] (WS), effects in heavy atoms such as optical rotation in allowed $M1$ transitions and circular dichroism (dependence of absorption on photon helicity) in forbidden $M1$ transitions may be observable.

An experiment to study the latter effect in the doubly forbidden $M1$ transition $6^2P_{1/2}$-$7^2P_{1/2}$ (292.7 nm) in atomic Tl vapor has been proposed.[3] The idea, originally suggested for the $6^2S_{1/2}$-$7^2S_{1/2}$ transition in Cs as well as the present Tl transition by Bouchiat and Bouchiat,[4] is that a short-range, parity-nonconserving, neutral weak interaction H_{PN} mixes the $6^2P_{1/2}$, $7^2P_{1/2}$ Tl states with $n^2S_{1/2}$ states. Thus the transition $6^2P_{1/2}$-$7^2P_{1/2}$, nominally $M1$ with amplitude

$$\mathfrak{M} = \langle 7^2P_{1/2}, m_J | M1 | 6^2P_{1/2}, m_J \rangle , \tag{1}$$

also contains a parity-nonconserving electric dipole component with amplitude

$$\mathcal{E}_{\text{PN}} = \langle 7^2P_{1/2}, m_J | E1 | 6^2P_{1/2}, m_J \rangle .$$

It can be shown that interference between $\mathfrak{M}$ and $\mathcal{E}_{\text{PN}}$ results in a dependence of the $6^2P_{1/2}$-$7^2P_{1/2}$ absorption rate W on right- (R) or left- (L) handed photon helicity:

$$\delta = \frac{W(R) - W(L)}{W(R) + W(L)} = \frac{2\,\text{Im}(\mathcal{E}_{\text{PN}})\mathfrak{M}}{|\mathfrak{M}|^2 + |\mathcal{E}_{\text{PN}}|^2} \approx \frac{2\,\text{Im}(\mathcal{E}_{\text{PN}})}{\mathfrak{M}} . \tag{2}$$

The "circular dichroism" δ can be detected by observing the fluorescence accompanying decay of the $7^2P_{1/2}$ state (see Fig. 1). The first step in that experiment was the determination of the $\mathfrak{M}1$ amplitude itself, the result being[3]

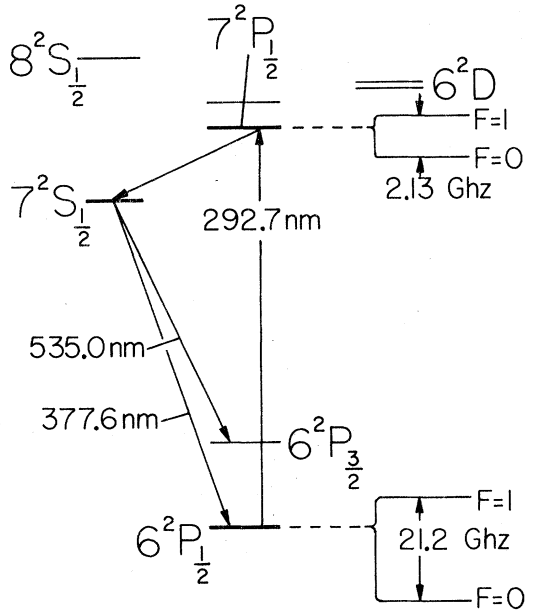

FIG. 1. Low-lying energy levels of the Tl atom (not to scale). The hyperfine structure splittings of $6^2P_{1/2}$, $7^2P_{1/2}$ states are shown. Absorption of the $6^2P_{1/2}$-$7^2P_{1/2}$ $M1$ photon (292.7 nm) is detected by observing fluorescence at 535 nm accompanying decay of the $7^2P_{1/2}$ state.

$$\mathfrak{M}_{\text{expt}} = (-2.11 \pm 0.30) \times 10^{-5} \mu_B \ , \tag{3}$$

where $\mu_B = |e|\hbar/2m_e c$. In that measurement and also in the experiment proposed to detect δ, use is made of the interference which occurs between $\mathfrak{M}$ and/or $\mathcal{E}_{\text{PN}}$ and the Stark-induced electric dipole amplitude $\mathcal{E}_S$ for $6\,^2P_{1/2}$-$7\,^2P_{1/2}$ transitions in an external electric field.

In this paper we present results of calculations of the atomic structure of Tl which are necessary in order to make useful comparisons between these experiments and the predictions of models of the neutral weak interaction. The thallium atom has 81 electrons with a ground-state electronic configuration: $1s^2 \ldots 5d^{10}6s^2 6p$. Our approach is to assume that all singly-excited TlI states of interest have the same inner electron configuration ($1s^2 \ldots 5d^{10}6s^2$, with total $L=0$, $S=0$) as that of the ground state, and differ only in the valence electron orbital. This approximation, while not strictly correct, is reasonable, since inner-shell ionization energies are at least several times larger than that of the $6p$ valence electron. It also has the obvious virtue of simplicity, since within such an approximation most properties of interest to us can be calculated from the valence-electron wave function, which is obtained by solving the Dirac equation numerically in a spherically symmetric potential, for all states of interest. We have chosen the potential

$$V(r) = -\frac{e^2(Z-1)}{\gamma(1+\eta r)^2} e^{-\gamma r} - \frac{e^2}{r} \ . \tag{4}$$

Without the exponential shielding factor $e^{-\gamma r}$, $V(r)$ is the "Tietz" potential,[5] which yields a good approximate solution to the Thomas-Fermi equation. The factor $e^{-\gamma r}$ is inserted to account for the exponential decrease of electron density for large r. Parameters η and γ are chosen so that the calculated and observed $6\,^2P_{1/2}$ and $7\,^2P_{1/2}$ energies agree.

We describe calculations of energy levels, allowed $E1$ oscillator strengths, and $P_{1/2}, S_{1/2}$ hyperfine-structure (hfs) splittings, all in good agreement with observations (see Sec. II). As is well known, the $6\,^2P_{3/2}$ hfs splitting is strongly affected by interconfiguration interaction, and a correction for this must be applied in order to obtain reasonable agreement with experiment (see Appendix A). Our calculation of $\mathfrak{M}$ (Sec. III) includes the one-electron relativistic contribution and corrections due to interconfiguration, hyperfine, and Breit interactions; the result is in agreement with the experimental value [Eq. (3)]. Our calculation of the Stark transition amplitudes $\mathcal{E}_S$ yields two second-order matrix elements α and β for linearly polarized excitation light parallel and perpendicular, respectively, to the applied static field E. The ratio β/α is in agreement with the experimental results of Chu, Commins, and Conti[3] (see Sec. V).

The satisfactory agreement between experiment and the calculations described in the previous paragraph provides confidence that our estimate of the parity-nonconserving amplitude $\mathcal{E}_{\text{PN}}$ should be reliable enough so that future experimental determinations of circular dichroism may yield useful tests of gauge models. For purposes of the present discussion, we present the analysis in terms of the WS model,[2] which describes low-energy strangeness-conserving neutral weak interactions in terms of an effective Hamiltonian density

$$\mathcal{H}(x) = (G/\sqrt{2}\,) J_\lambda(x) J^\lambda(x) \ , \tag{5}$$

where G is the Fermi coupling constant of weak interactions $G = 3 \times 10^{-12}$ in units ($\hbar = m_e = c = 1$) used throughout. The current $J^\lambda(x)$ has both hadronic and leptonic parts, the former being expressible as

$$J^\lambda_{\text{had}} = V^{\lambda,0} + A^{\lambda,0} - 2\sin^2\theta_W J^{\lambda,\text{EM}} \ , \tag{6}$$

where $V^{\lambda,0}$ is the I_3 component of the strangeness-conserving hadronic vector current, $A^{\lambda,0}$ is the neutral $\Delta S = 0$ hadronic axial current, $J^{\lambda,\text{EM}}$ is the EM current, and θ_W is the so-called "Weinberg" angle, which is given by $\sin^2\theta_W \cong 0.3$. That portion of the neutral leptonic current involving e^- is

$$J^{\text{lept},e^-}_\lambda = -\tfrac{1}{2}[(1 - 4\sin^2\theta_W)\bar{\Psi}_e \gamma_\lambda \Psi_e + \bar{\Psi}_e \gamma_\lambda \gamma_5 \Psi_e] \ , \tag{7}$$

where Ψ_e is the electron field operator. The first and second terms on the right-hand side (RHS) are respectively vector and axial-vector currents. We are interested in those portions of $\mathcal{H}(x)$ which are pseudoscalar, not scalar; thus we consider the product of the axial portion of $J^{\text{lept},e^-}_\lambda$ and the vector portion of J^λ_{had}. (The other pseudoscalar term corresponding to the product of the vector part of $J^{\text{lept},e^-}_\lambda$ and the axial part of J^λ_{had} gives a much smaller contribution since it is proportional to total nuclear spin, and for a heavy nucleus most of the nucleon spins cancel in pairs.) Ignoring this latter portion, we find

$$\mathcal{H}^{\text{PN}}(x) \cong -(G/\sqrt{2}\,)\bar{\Psi}_e \gamma_\lambda \gamma_5 \Psi_e \times (V^{\lambda,0} - 2\sin^2\theta_W J^{\lambda,\text{EM}}) \ . \tag{8}$$

Taking matrix elements of $\mathcal{H}^{\text{PN}}(x)$ for the static limit of the nucleus, we obtain the matrix element of the effective Hamiltonian

$$\langle H^{\text{PN}} \rangle = (-GQ_W/2\sqrt{2}\,)\psi^*_2(\vec{x})\gamma_5\psi_1(\vec{x})\big|_{x=0} \ , \tag{9}$$

where

$$Q_W = (1 - 4\sin^2\theta_W)Z - N \tag{10}$$

and $\psi_1(\vec{x})$ and $\psi_2(\vec{x})$ are Dirac wave functions corresponding to states of opposite parity, and "$x=0$" indicates the product is averaged over the nuclear volume. In fact, only $P_{1/2}$ and $S_{1/2}$ states yield non-negligible matrix elements. Equation (9) is derived from the WS model. However, other gauge models with parity nonconservation would lead to the same expression with only Q_W of Eq. (10) being model dependent. In most cases $|Q_W| \sim Z$. In Sec. IV we use Eq. (9) to calculate $\mathcal{E}_{\mathrm{PN}}$. Finally, Sec. VI contains an estimate of parity-nonconserving effects for transitions in Tl other than $6\,^2P_{1/2}$-$7\,^2P_{1/2}$.

II. THALLIUM WAVE FUNCTIONS IN THE ONE-ELECTRON CENTRAL-FIELD APPROXIMATION

A. Construction of wave functions

The Dirac equation is

$$(\vec{\alpha}\cdot\vec{p}+\beta-eV)\psi=(1-E_I)\psi\,, \tag{11}$$

where E_I is the valence-electron ionization energy [$(1-E_I)$ is the total electron energy including rest mass], and $\vec{\alpha}$ and β are the usual Dirac matrices. We write

$$\psi=\begin{pmatrix} f(r)/r\ \chi^{\mu}_{\kappa} \\ ig(r)/r\ \chi^{\mu}_{-\kappa}\end{pmatrix}. \tag{12}$$

As usual, $\kappa=\mp(j+\frac{1}{2})$ for even (odd) parity states, the $\chi^{\mu}_{\pm\kappa}$ are two-component spin-angular-momentum functions[6] given by

$$\chi^{\mu}_{\kappa}(\theta,\phi)=\begin{pmatrix} C(\tfrac{1}{2},l,j;\tfrac{1}{2},\mu-\tfrac{1}{2},)\ Y_l^{\mu-1/2}(\theta,\phi) \\ C(\tfrac{1}{2},l,j;-\tfrac{1}{2},\mu+\tfrac{1}{2},\mu)\ Y_l^{\mu+1/2}(\theta,\phi)\end{pmatrix}, \tag{13}$$

the C's are Clebsch-Gordan coefficients, $\mu\equiv m_j$, $l=|\kappa+\frac{1}{2}|$, and the Y's are spherical harmonics. Equation (12) reduces to the two coupled radial equations

$$\begin{aligned}\frac{df}{dr}&=-\frac{\kappa}{r}f+[2-E_I-V(r)]g\,,\\ \frac{dg}{dr}&=\frac{\kappa}{r}g+[E_I+V(r)]f\,.\end{aligned} \tag{14}$$

Following the procedure used by Schwartz[7] to calculate hyperfine-structure splittings in Tl and other heavy atoms, we choose for $V(r)$ the modified Tietz potential of Eq. (4). Parameters η and γ are chosen so that calculated and observed $6\,^2P_{1/2}$ and $7\,^2P_{1/2}$ energies agree. The fitting procedure is as follows:

(i) For very small r ($r\leq r_0=0.02\hbar/m_ec=0.02$), i.e., for r within the nuclear radius r_0, one of the following three potentials is chosen:

(a) $V(r)=-Ze^2/r$ (point nucleus),

(b) $V(r)=-Ze^2/r_0$ (constant potential),

(c) $V(r)=(Ze^2/2r_0)(r^2/r_0^2-3)$ (constant nuclear charge density).

The initial wave-function values for this region are generated using a power-series expansion to solve Eqs. (14).

(ii) For $r\geq r_0$ Eqs. (14) for $f(r)$ and $g(r)$ are integrated numerically stepwise using a fourth-order Runge-Kutta method.[8] Approximately 5000 intervals of length increasing from 0.001Å to 2.0Å are used.

(iii) The eigenvalue condition is that $\lim_{r\to\infty}f(r)=0$. The energy E_I in Eqs. (14) is varied to insure that this condition is satisfied.

The energy spectrum does not depend strongly on the choice of potential in step (i). Of all the quantities computed below, only the weak electron-nucleus interaction depends significantly on this choice, and for that quantity the dependence is only ~10%. The number of intervals can be reduced substantially without significant loss of precision except for calculation of the forbidden $M1$ transition (see Sec. III); however, this reduction would provide no economic advantage on the LBL CDC 7600 computer. The calculation procedure can be reversed by choosing an asymptotic form for f and g at large r, and integrating stepwise toward $r=0$. This yields the same states as the procedure actually used, but is less convenient for calculation of $\mathcal{E}_{\mathrm{PN}}$.

The values of η and γ chosen for most calculations are

$$\begin{aligned}\eta&=2.5937a_0^{-1}=355.43\text{Å}^{-1}\,,\\ \gamma&=0.2579a_0^{-1}=35.34\text{Å}^{-1}\,.\end{aligned} \tag{15}$$

Numerical values of f/r and g/r vs r are given for several states in Table I. These values are chosen to yield agreement between calculated and observed $6\,^2P_{1/2}$, $7\,^2P_{1/2}$ energy levels to within 0.1%. Other low-lying $S_{1/2}$, $D_{1/2}$, $P_{1/2}$, and $P_{3/2}$ energy levels are calculated, and these all agree with observations to within 2%. Table II includes a comparison of calculated and observed energy levels.

B. Hyperfine structure

The one-electron central-field (OECF) wave functions described above can be used to calculate hyperfine-structure splittings for comparison with experimental values. This comparison provides a reasonably sensitive test of the accuracy of calculations of $\mathcal{E}_{\mathrm{PN}}$ since both the latter and the hfs depend on values of the wave functions near the origin. The perturbation Hamiltonian for hfs is

TABLE I. Dirac radial functions f/r and g/r for selected states.

r	$6P_{1/2}$		$6P_{3/2}$		$7P_{1/2}$		$7S_{1/2}$		$6D_{3/2}$	
(Å)	$f(r)/r$	$g(r)/r$	$f(r)/r$	$g(r)/r$	$f(r)/r$	$g(r)/r$	$f(r)/r$	$g(r)/r$	$f(r)/r$	$g(r)/r$
0.02	2.383×10^{-3}	5.985×10^{-3}	4.014×10^{-5}	-4.454×10^{-6}	8.391×10^{-4}	2.107×10^{-3}	8.491×10^{-3}	-2.090×10^{-3}	1.582×10^{-7}	1.329×10^{-6}
0.12	1.678	3.970	2.004×10^{-4}	-3.040×10^{-5}	5.908	1.398	5.782	−1.915	1.339×10^{-6}	6.675×10^{-6}
0.32	1.739	3.000	4.608	-7.035	6.122	1.056	4.146	−1.459	4.416	1.555×10^{-5}
0.62	1.920	2.300	7.678	-1.184×10^{-4}	6.761	8.101×10^{-4}	2.889	−1.111	1.088×10^{-5}	2.643
1.42	2.177	1.329	1.272×10^{-3}	−2.022	7.667	4.146	1.137	-6.232×10^{-4}	3.568	4.641
2.40	2.116	7.010×10^{-4}	1.491	−2.483	7.452	2.469	1.178×10^{-4}	−3.113	7.335	5.913
4.40	1.438	1.170	1.272	−2.431	5.492	4.119×10^{-5}	−5.188	−3.300	1.479×10^{-4}	6.307
6.40	6.498×10^{-4}	-7.624×10^{-5}	7.541×10^{-4}	−1.862	2.288	−2.686	−4.468	4.905×10^{-5}	1.988	5.373
8.40	3.484×10^{-5}	-1.181×10^{-4}	2.579	−1.223	1.221×10^{-5}	−4.159	−2.095	5.933	2.212	4.072
10.40	-3.545×10^{-4}	−1.029	−1.120	-6.774×10^{-5}	-1.249×10^{-4}	−3.623	8.735×10^{-6}	4.549	2.192	2.812
12.40	−5.474	-7.090×10^{-5}	−3.412	−2.690	−1.928	−2.496	1.557×10^{-4}	2.674	1.999	1.748
14.40	−5.949	−3.882	−4.501	8.953×10^{-7}	−2.045	−1.366	2.296	1.035	1.698	9.173×10^{-6}
18.40	−4.428	6.076×10^{-6}	−4.693	1.802×10^{-5}	−1.559	2.152×10^{-6}	2.224	-9.239×10^{-6}	9.727×10^{-5}	−1.242
24.00	-7.630×10^{-5}	2.738×10^{-5}	−1.759	2.833	-2.673×10^{-5}	9.650	7.174×10^{-5}	-1.448×10^{-5}	5.380×10^{-6}	−6.513
44.00	2.924×10^{-4}	5.932×10^{-7}	2.646	-4.910×10^{-6}	1.028×10^{-4}	1.943×10^{-7}	-1.331×10^{-4}	2.688×10^{-6}	-8.549×10^{-5}	−2.090
64.00	-2.830×10^{-5}	-7.414×10^{-6}	4.584×10^{-5}	−6.436	-1.038×10^{-5}	-2.617×10^{-6}	2.078×10^{-5}	3.321	−2.523	1.021
84.00	-2.000×10^{-4}	−4.208	-1.308×10^{-4}	−1.843	−7.059	−1.472	9.622	5.844×10^{-7}	2.586	1.371
120.00	−1.161	4.658×10^{-7}	−1.616	1.631	−5.575	1.881×10^{-7}	5.576	-1.094×10^{-6}	5.549	7.503×10^{-7}
220.00	1.172	1.125×10^{-6}	6.475×10^{-5}	5.257×10^{-7}	4.251	3.866	−6.797	-8.433×10^{-8}	2.296	-3.148×10^{-8}
320.00	1.497	3.754×10^{-7}	1.230×10^{-4}	−1.560	4.866	8.494×10^{-8}	−4.468	2.076×10^{-7}	-5.243×10^{-6}	-1.241×10^{-7}
420.00	1.174	9.062×10^{-8}	1.107	−2.489	2.984	−3.331	-5.083×10^{-6}	1.712	-1.971×10^{-5}	−1.211
620.00	5.470×10^{-5}	−4.168	6.172×10^{-5}	−1.546	-5.002×10^{-6}	−7.184	3.604×10^{-5}	4.523×10^{-8}	−3.048	-8.423×10^{-8}
820.00	2.313	−2.271	3.007	-7.456×10^{-8}	-2.191×10^{-5}	−5.060	4.121	-9.513×10^{-9}	−3.144	−5.262
1020.00	9.481×10^{-6}	−1.205	1.400	−5.061	−2.651	−2.763	3.375	-2.372×10^{-8}	−2.804	−3.074
1420.00	1.531	-2.444×10^{-9}	2.852×10^{-6}	-6.770×10^{-9}	−2.074	-3.184×10^{-9}	1.617	−1.735	−1.865	-8.203×10^{-9}
1820.00	2.402×10^{-7}	-4.271×10^{-10}	3.188×10^{-7}	−1.300	−1.203	2.811	6.387×10^{-6}	-7.867×10^{-9}	−1.075	-7.861×10^{-10}
2600.00	6.195×10^{-8}	-1.224×10^{-11}	2.155×10^{-8}	-4.915×10^{-11}	-2.960×10^{-6}	1.777	8.224×10^{-7}	−1.131	-2.933×10^{-6}	9.397
3100.00	5.710×10^{-10}	-1.219×10^{-12}	3.197×10^{-9}	-4.917×10^{-12}	−1.067	7.784×10^{-10}	2.025	-2.884×10^{-10}	−1.160	5.451
3600.00					-3.634×10^{-7}	2.984	4.788×10^{-8}	-6.975×10^{-11}	-4.377×10^{-7}	2.529
4100.00					−1.189	1.058	1.109	−1.617	−1.593	1.051
4600.00					-3.776×10^{-8}	3.563×10^{-11}	2.825×10^{-9}	-3.256×10^{-12}	-5.638×10^{-8}	4.083×10^{-11}
5600.00					-3.316×10^{-9}	3.946×10^{-12}			-6.639×10^{-9}	5.435×10^{-12}
6600.00									-7.359×10^{-10}	6.509×10^{-13}

TABLE II. Energy levels and hyperfine structure splittings.

Spectroscopic level designation	Fitted energy level (ionization energy, $m_e c^2 = 1$)	Spectroscopic energy level[a]	Valence-electron hyperfine splitting (GHz)	Observed hyperfine splitting (GHz)
$6p\,^2P_{1/2}$	1.1939×10^{-5}	1.1953×10^{-5}	21.8	21.3[b]
$6p\,^2P_{3/2}$	9.8745×10^{-6}	1.0062×10^{-5}	3.27	0.528[c]
$7p\,^2P_{1/2}$	3.6756×10^{-6}	3.6648×10^{-6}	2.71	2.13[d]
$7p\,^2P_{3/2}$	3.3937×10^{-6}	3.4219×10^{-6}	0.494	0.62[d]
$8p\,^2P_{1/2}$	1.9199×10^{-6}	1.9158×10^{-6}	0.989	0.79[e]
$8p\,^2P_{3/2}$	1.8155×10^{-6}	1.8254×10^{-6}	0.187	0.26[e]
$7s\,^2S_{1/2}$	5.4164×10^{-6}	5.5289×10^{-6}	14.3	12.4[b]
$8s\,^2S_{1/2}$	2.5169×10^{-6}	2.5521×10^{-6}	4.32	
$9s\,^2S_{1/2}$	1.4650×10^{-6}	1.4796×10^{-6}	1.90	
$10s\,^2S_{1/2}$	9.594×10^{-7}	9.6260×10^{-7}	1.01	
$11s\,^2S_{1/2}$	6.772×10^{-7}	6.811×10^{-7}	0.59	

[a] C. E. Moore, *Atomic Energy Levels*, NBS Circ. No. 467 (U.S. GPO, Washington, D. C., 1958), Vol. III.
[b] A. Gallagher and A. Lurio, Phys. Rev. 136, A87 (1964).
[c] G. Gould, Phys. Rev. 101, 1828 (1956).
[d] A. Flusberg, T. Mossberg, and S. R. Hartmann, Phys. Lett. 55A, 403 (1976).
[e] A. N. Odintsov, Opt. Spektrosk. 9, 142 (1960) [Opt. Spectrosc. (USSR) 9, 75 (1960)].

$$H_{\rm HFS} = e\vec{\alpha}\cdot\vec{A} = e\vec{\alpha}\cdot(\vec{m}_n\times\vec{r}/r^3) = e\vec{m}_n\cdot(\vec{r}\times\vec{\alpha}/r^3)\ , \tag{16}$$

where $\vec{m}_n = g_n\mu_n\vec{I}$ is the nuclear magnetic moment operator, μ_n is the nuclear Bohr magneton, and $I=\frac{1}{2}$ is the spin for both stable thallium isotopes, ^{203}Tl and ^{205}Tl. Also, $g_n(^{203}\mathrm{Tl}) = 3.223$ and $g_n(^{205}\mathrm{Tl}) = 3.255$[9]; in our calculations these are averaged to $g_n = 3.24$. It can then be shown that the hfs energy splittings are given in first order by[6]

$$\Delta W = eg_n\mu_n(J+\tfrac{1}{2})[\,8\kappa/(4\kappa^2-1)]R\ , \tag{17}$$

where

$$R = \int_0^\infty \frac{fg}{r^2}\,dr\ . \tag{18}$$

Table II includes a list of hfs splittings calculated for the various energy levels, together with experimental values where these are available. The discrepancies are not due to major defects in the wave functions, but rather to interconfiguration interaction, which is known to have an especially large effect on the $6\,^2P_{3/2}$ state. This is demonstrated in Appendix A which contains an estimate of interconfiguration interaction for $6p$ electron states. Although the effect on the $6\,^2P_{3/2}$ hfs splitting is large it can be shown that interconfiguration interaction corrections to $\mathcal{E}_{\rm PN}$ are relatively small.

C. Fine structure

Another test of the wave function for small r is the fine-structure splitting $\Delta E = E(j=l+\frac{1}{2}) - E(j=l-\frac{1}{2})$ for $l\neq 0$. Nonrelativistically,

$$\Delta E = (l+\tfrac{1}{2})\langle nl\,|\,\frac{1}{r}\frac{dV}{dr}\,|nl\rangle\ .$$

In a relativistic calculation such as ours, the fine structure is part of the unperturbed Hamiltonian, and the calculated fine structure is simply the difference between calculated $j=l+\frac{1}{2}$ and $j=l-\frac{1}{2}$ energy levels. Comparison of these differences with observed energy differences from Table II for P states yields discrepancies $\lesssim 15\%$.

D. Allowed electric dipole transitions

We also calculate electric dipole radial integrals and transition strengths using the OECF wave functions. In the relativistic notation of Berestetskii, Lifschitz, and Pitaevskii,[10] the transition matrix element is

$$V_{fi} = e\int d^3\vec{r}\,j^\mu_{fi}(\vec{r})A^*_\mu(\vec{r})\ , \tag{19}$$

where $j^\mu_{fi}(r) = \bar{\psi}_f\gamma^\mu\psi_i$ is written in terms of the initial and final Dirac wave functions ψ_i, ψ_f, γ^μ are the standard 4×4 matrices, and $A_\mu(\vec{r})$ is the 4-vector potential. In the long-wavelength approximation for an electric multipole field of order

J,M, we have

$$A_\mu(\vec{r})=(A_0(\vec{r}),0,0,0)\ ,$$

$$A_0(r)=-\int\frac{d^3\vec{k}}{(2\pi)^3}\left(\frac{J+1}{J}\right)^{1/2}\frac{4\pi^2}{\omega^{3/2}}\times\delta(|\vec{k}|-\omega)Y_J^M(\vec{k}/\omega)\cdot e^{i\vec{k}\cdot\vec{r}}$$

$$\cong r^J(-1)^{M+1}i^J\left(\frac{J+1}{J}\right)^{1/2}\times\frac{2\omega^{J+1/2}}{(2J+1)!!}Y_J^M(\vec{r}/r)\ . \tag{20}$$

For $E1$ radiation, this becomes

$$A_0(\vec{r})=(-1)^{M+1}ir\tfrac{2}{3}\sqrt{2}\ \omega^{3/2}Y_1^M(\vec{r}/r)\ . \tag{21}$$

Combining Eqs. (19) and (21), we obtain

$$V_{fi}^{1,M}=(-1)i\omega^{3/2}\frac{2\sqrt{2}}{3}\times\int d^3\vec{r}\,\psi_f^*(\vec{r})rY_1^{M*}(\vec{r}/r)\psi_i(\vec{r})\ . \tag{22}$$

The spontaneous emission rate A is given by

$$A_{fi}=2\pi\langle V_{fi}^2\rangle\ ,$$

where $\langle V_{fi}^2\rangle$ is V_{fi}^2 summed over photon states and final electron states (j_f,m_f), and averaged over initial electron states (j_i,m_i). For OECF wave functions the angular integration is easily separated, and we find the following:

Transition	A coefficient
$S_{1/2}\to P_{1/2}, D_{3/2}\to P_{1/2}$	$\frac{4}{9}e^2\omega^3\langle r\rangle_{fi}^2$
$S_{1/2}\to P_{3/2}$	$\frac{8}{9}e^2\omega^3\langle r\rangle_{fi}^2$
$D_{3/2}\to P_{3/2}$	$\frac{4}{45}e^2\omega^3\langle r\rangle_{fi}^2$
$D_{5/2}\to P_{3/2}$	$\frac{8}{15}e^2\omega^3\langle r\rangle_{fi}^2$

where ω is the observed energy difference between initial and final states, and $\langle r\rangle_{fi}=\int r(f_ff_i+g_fg_i)dr$. The signs of these radial integrals are fixed by the convention that $f(r)>0$ as $r\to 0$ for every state. In Table III, the radial integrals $\langle r\rangle_{fi}$ and calculated A coefficients for $nD\to 6P$ and $nS\to 6P$ transitions are listed, together with observed A coefficients for the same transitions as determined by Gallagher and Lurio.[11] The agreement between theory and experiment is generally good, the discrepancy in the transition rates typically being $\lesssim 20\%$. This corresponds to a discrepancy in the radial integrals of $\lesssim 10\%$, and reveals that our wave functions are reasonably accurate in the range $r\geq 2a_0$.

The oscillator strengths F_{fi} are defined by

$$F_{fi}=\left(\frac{2J_f+1}{2J_i+1}\right)\frac{A_{if}}{2e^2\omega^2}\ , \tag{23}$$

TABLE III. Allowed $E1$ transition rates.

Transition	A coefficient (10^7 sec^{-1}) Ref. 11	A coefficient (10^7 sec^{-1}) This work	Radial integral $\langle r\rangle_{fi}$ (Å)	Oscillator strength This work	Oscillator strength Ref. 12
$7\,^2S_{1/2}$-$6\,^2P_{1/2}$	6.25 ±0.31	5.78	294.1	0.124	0.123
$8\,^2S_{1/2}$-$6\,^2P_{1/2}$	1.78 ±0.16	1.75	91.5	0.017 5	0.017 2
$9\,^2S_{1/2}$-$6\,^2P_{1/2}$	0.78 ±0.10	0.777	51.8	0.006 25	0.006 16
$10\,^2S_{1/2}$-$6\,^2P_{1/2}$	•••	0.412	35.1	0.003 01	0.002 95
$11\,^2S_{1/2}$-$6\,^2P_{1/2}$	0.31 ±0.06	0.244	26.0	0.001 70	0.001 67
$7\,^2S_{1/2}$-$6\,^2P_{3/2}$	7.05 ±0.32	8.30	422.1	0.178	0.162
$8\,^2S_{1/2}$-$6\,^2P_{3/2}$	1.73 ±0.18	2.30	103.9	0.018 0	0.017 2
$9\,^2S_{1/2}$-$6\,^2P_{3/2}$	0.80 ±0.08	1.01	56.3	0.006 05	0.005 9
$10\,^2S_{1/2}$-$6\,^2P_{3/2}$	0.57 ±0.06	0.534	37.5	0.002 85	0.002 86
$6\,^2D_{3/2}$-$6\,^2P_{1/2}$	12.6 ±1.0	16.04	−307.7	0.368	0.40
$7\,^2D_{3/2}$-$6\,^2P_{1/2}$	4.4 ±0.5	6.39	−154.8	0.109	0.121
$8\,^2D_{3/2}$-$6\,^2P_{1/2}$	1.89 ±0.3	3.19	−99.8	0.043 4	0.053
$9\,^2D_{3/2}$-$6\,^2P_{1/2}$	0.98 ±0.22	1.82	−71.9	0.025 7	0.028
$10\,^2D_{3/2}$-$6\,^2P_{1/2}$	0.58 ±0.15	1.14	−55.2	0.015 6	0.017
$6\,^2D_{3/2}$-$6\,^2P_{3/2}$	2.20 ±0.23	2.88	−419.6	0.053 8	0.052
$7\,^2D_{3/2}$-$6\,^2P_{3/2}$	0.76 ±0.08	1.01	−186.9	0.012 9	0.013 6
$8\,^2D_{3/2}$-$6\,^2P_{3/2}$	0.37 ±0.04	0.498	−117.5	0.005 49	0.005 6
$9\,^2D_{3/2}$-$6\,^2P_{3/2}$	0.19 ±0.02	0.279	−83.0	0.002 85	0.002 9
$6\,^2D_{5/2}$-$6\,^2P_{3/2}$	12.4 ±1.5	16.3	−405.6	0.489	0.46
$7\,^2D_{5/2}$-$6\,^2P_{3/2}$	4.2 ±0.5	6.06	−186.9	0.116	0.12
$8\,^2D_{5/2}$-$6\,^2P_{3/2}$	1.7 ±0.2	2.96	−116.9	0.048 9	0.051

TABLE IV. Oscillator strengths for nS-$7P$, nD-$7P$ transitions.

Transition	Radial integral $\langle r\rangle_{fi}$ (Å)	Oscillator strength This work	Ref. 12
$7\,^2S_{1/2}$-$7\,^2P_{1/2}$	−1072.6	0.315	0.440
$8\,^2S_{1/2}$-$7\,^2P_{1/2}$	991.6	0.241	0.258
$9\,^2S_{1/2}$-$7\,^2P_{1/2}$	219.5	0.023 4	0.021 9
$10\,^2S_{1/2}$-$7\,^2P_{1/2}$	114.3	0.007 84	0.007 41
$11\,^2S_{1/2}$-$7\,^2P_{1/2}$	75.1	0.002 77	0.003 42
$7\,^2S_{1/2}$-$7\,^2P_{3/2}$	−1007.8	0.476	0.440
$8\,^2P_{1/2}$-$7\,^2P_{3/2}$	1240.2	0.297	0.294
$9\,^2S_{1/2}$-$7\,^2P_{3/2}$	202.2	0.017 6	0.016 4
$10\,^2S_{1/2}$-$7\,^2P_{3/2}$	100.4	0.005 50	0.005 42
$6\,^2D_{3/2}$-$7\,^2P_{1/2}$	1321.4	0.369	0.340
$7\,^2D_{3/2}$-$7\,^2P_{1/2}$	−489.2	0.202	0.248
$8\,^2D_{3/2}$-$7\,^2P_{1/2}$	−254.2	0.073 3	0.085 0
$9\,^2D_{3/2}$-$7\,^2P_{1/2}$	−165.3	0.035 2	0.039 9
$10\,^2D_{3/2}$-$7\,^2P_{1/2}$	−120.0	0.019 9	0.022 3
$6\,^2D_{3/2}$-$7\,^2P_{3/2}$	1328.0	0.015 2	0.016 6
$7\,^2P_{3/2}$-$7\,^2P_{3/2}$	−729.8	0.039 6	0.041 8
$8\,^2D_{3/2}$-$7\,^2P_{3/2}$	−331.0	0.009 37	0.011 6
$9\,^2D_{3/2}$-$7\,^2P_{3/2}$	−204.9	0.004 95	0.005 06

where J_i and J_f are the initial and final total electronic angular momenta. These quantities have previously been calculated by Anderson *et al.*[12] by a method similar to ours (one-electron Dirac wave function and central potential). Table III includes a comparison of their calculated oscillator strengths with ours for $nD \to 6P$ and $nS \to 6P$ transitions. Table IV gives the same comparison for $7P \to nS$ and $7P \to nD$ transitions, the radial integrals for which are needed in evaluation of $\mathcal{E}_{PN}$ and $\mathcal{E}_S$ (see Secs. IV and V). Our calculated oscillator strengths and those of Anderson *et al.* are nearly identical, which suggests that the discrepancies ($\lesssim 20\%$) between calculated and observed values are due to a failure of the OECF approximation, rather than merely to an inadequate central potential. Thus to obtain more accurate results it may be necessary to go beyond the simple OECF model.

III. MAGNETIC DIPOLE TRANSITION RATES

A. Relativistic contribution

The relativistic contribution to $\mathfrak{M}$ arises from the transition matrix element[10]

$$V_{fi} = ie\sqrt{2\omega}\int d^3r\,\psi_f^*(\vec{r})\vec{\alpha}\psi_i(\vec{r})\cdot\left(\frac{\vec{r}\times\vec{\nabla}}{\sqrt{2}}Y_{1m}^*\right)g_1(kr)\,, \tag{24}$$

where $g_1(kr) = (\pi/2kr)^{1/2}J_{3/2}(kr)$ is a spherical Bessel function. Using Eq. (12) for ψ_i and ψ_f which are both $P_{1/2}$ states, employing

$$\vec{\alpha} = \begin{pmatrix} 0 & \vec{\sigma} \\ \vec{\sigma} & 0 \end{pmatrix}$$

and $(\vec{\sigma}\cdot\vec{r}/r)\chi_1^\mu = -\chi_{-1}^\mu$, and utilizing the anticommutation of $\vec{\sigma}\cdot\vec{r}/r$ and $\vec{\sigma}\cdot\vec{\nabla}Y_{1m}$, we obtain

$$V_{fi} = -ie\sqrt{2\omega}\int dr\,g_1(kr)(f_fg_i+f_ig_f) \times\int r\,d\Omega\,\chi_{-1}^{\mu_f*}\vec{\sigma}\cdot\vec{\nabla}Y_{1m}^*\chi_{-1}^{\mu_i}\,. \tag{25}$$

We rewrite this as

$$V_{fi} = (-1)^m i(2/3\pi)^{1/2}\omega^{3/2}\vec{\mu}_{fi}\cdot\hat{\epsilon}_m\,, \tag{26}$$

where $\hat{\epsilon}_m$ is the spherical unit vector

$$\hat{\epsilon}_m = \vec{\nabla}[(4\pi/3)^{1/2}r\,Y_{1m}] \tag{27}$$

and

$$\vec{\mu}_{fi}\cdot\hat{\epsilon}_m = -e\int dr\,\frac{g_1(kr)}{\omega}(f_fg_i+g_ff_i) \times\int d\Omega\,\chi_{-1}^{\mu_f*}\vec{\sigma}\cdot\vec{\nabla}(4\pi/3)^{1/2}rY_{1m}\chi_{-1}^{\mu_i} \tag{28}$$

for $P_{1/2}\to P_{1/2}$ transitions. The expression for $\vec{\mu}_{fi}\cdot\hat{\epsilon}_m$ in the case of $S_{1/2}$-$S_{1/2}$ transitions is the same except for a change in sign.

To find the transition rate

$$A = 2\pi\langle|V_{fi}|\rangle^2 = \tfrac{4}{3}\omega^3\langle|\vec{\mu}_{fi}\cdot\hat{\epsilon}_m|^2\rangle\,, \tag{29}$$

we sum over final and average over initial states to obtain

$$A = 4\omega^3e^2\left|\int\frac{g_1(kr)}{\omega}(f_fg_i+g_ff_i)\,dr\right|^2. \tag{30}$$

This formula was previously obtained by Johnson[13] for the $2\,^2S_{1/2}$-$1\,^2S_{1/2}$ $M1$ transition in hydrogen. The result is also valid for allowed $\frac{1}{2}$-$\frac{1}{2}$ transitions. In this case $\vec{\mu}_{fi}$ of Eq. (28) approaches the familiar

$$\vec{\mu}_{fi} = \int\psi_f^*\left(\frac{e}{2}\vec{L}+\mu_e\frac{\vec{S}}{S}\right)\psi_i\,d^3r \tag{31}$$

in the nonrelativistic limit. This expression vanishes if the radial parts of ψ_i and ψ_f are orthogonal.

We use our OECF radial wave functions for $6\,^2P_{1/2}, 7\,^2P_{1/2}$ states to compute the result

$$\mathfrak{M}_{rel} = -e\int\frac{g_1(kr)}{\omega}(f_ig_f+g_if_f)\,dr = -1.757\times10^{-5}\mu_B\,. \tag{32}$$

The extremely small size of this matrix element implies that relatively large corrections might occur due to interconfiguration mixing, hyperfine mixing, and the Breit interaction.

B. Interconfiguration interaction correction

Electrostatic interaction of the outer electron with excited core states alone (as in Appendix A) does not directly effect the $M1$ transition rate, since it mixes only those states having the same total L and S ($^2P_{1/2}$ in Tl).[14] However, in second order, spin-orbit coupling allows an admixture of different L, S atomic states (e.g., $^4P_{1/2}$ in Tl) and this admixture can give rise to a finite $M1$ amplitude even in the nonrelativistic limit.

A consistent fourth-order treatment is necessary; the calculation which follows is similar to that done by Phillips for corrections to g_J(Cs).[14] Since the ground configuration of Tl is $1s^2 \ldots 5d^{10} 6s^2 6p$, we only consider the effects of $6s$-electron excitation (the correction due to $5d$ excitation turns out to be smaller). The unperturbed states are

$$\begin{aligned} \psi_6 &\equiv \psi(6\,^2P_{1/2}) = 6s^2(^1S_0)6p\,^2P_{1/2} \ , \\ \psi_7 &\equiv \psi(7\,^2P_{1/2}) = 6s^2(^1S_0)7p\,^2P_{1/2} \ . \end{aligned} \tag{33}$$

The first-order perturbation is the electrostatic interaction and the perturbing states considered are

$$\begin{aligned} \Phi_6 &= 6s7s(^3S_1)6p\,^2P_{1/2} \ , \\ \Phi_7 &= 6s7s(^3S_1)7p\,^2P_{1/2} \ . \end{aligned} \tag{34}$$

Thus the perturbed states are

$$\begin{aligned} \psi_6' &= \psi_6 + \alpha_6\Phi_6 + \alpha_7\Phi_7 \ , \\ \psi_7' &= \psi_7 + \beta_6\Phi_6 + \beta_7\Phi_7 \ , \end{aligned} \tag{35}$$

where α_6, α_7, β_6, β_7 are calculated by first-order perturbation theory, and antisymmetrization of the total wave function is taken into account. For example,

$$\alpha_6 = -(3/2)^{1/2} G_1(6s, 6p; 7s, 6p)/\Delta E \ ,$$

where $G_1(6s, 6p; 7s, 6p)$ is the exchange electrostatic integral, $\Delta E = E(\Phi_6) - E(\psi_6)$, and $E(\Phi_6)$ is a fictitious energy calculated for a $6s7s6p$ configuration in the potential of Eq. (4). Numerical computation gives

$$\alpha_6 = -0.010, \ \alpha_7 = +0.023, \ \beta_6 = 0.094, \ \beta_7 = 0.006 \ . \tag{36}$$

The $6s7s(^3S_1)mp^2P_{1/2}$ states are now mixed with states

$$\Phi_n'(^4P_{1/2}) = 6s7s(^3S_1)n'p^4P_{1/2} \tag{37}$$

by spin-orbit interaction. We employ the perturbation Hamiltonian

$$H' = \sum_i \xi_i \cdot \vec{L}_i \cdot \vec{S}_i = \frac{1}{2}\sum_i \left(\frac{1}{r}\frac{\partial V}{\partial r}\right)_i \vec{L}_i \cdot \vec{S}_i \tag{38}$$

and rewrite our wave functions as

$$\begin{aligned} \psi_6' = \psi_6 &+ \alpha_6[\Phi_6 + a_6\Phi_6'(^4P_{1/2}) + a_7\Phi_7'(^4P_{1/2})] \\ &+ \beta_6[\Phi_7 + b_6\Phi_6'(^4P_{1/2}) + b_7\Phi_7'(^4P_{1/2})] \end{aligned} \tag{39}$$

and

$$\begin{aligned} \psi_7' = \psi_7 &+ \alpha_7[\Phi_6 + c_6\Phi_6'(^4P_{1/2}) + c_7\Phi_7'(^4P_{1/2})] \\ &+ \beta_7[\Phi_7 + d_6\Phi_6'(^4P_{1/2}) + d_7\Phi_7'(^4P_{1/2})] \ . \end{aligned} \tag{40}$$

The coefficients $a_6, \ldots, d_7$ are calculated from the observed P-state fine-structure splitting. For example,

$$a_6 = -\frac{2\sqrt{2}}{9}\frac{[E(6^2P_{3/2}) - E(6^2P_{1/2})]}{\Delta E} \ , \tag{41}$$

where $\Delta E = E(\psi_6) - E(\Phi_6')$. We find $a_6 = +0.033$, $a_7 = +0.0081$, $b_6 = +0.012$, $b_7 = +0.0029$, $c_6 = +0.061$, $c_7 = +0.012$, $d_6 = +0.022$, $d_7 = 0.0043$. The interconfiguration interaction correction is now computed from Eqs. (39) and (40) by means of the formula

$$\mathfrak{M}_{II} = \langle \Psi_6' | M1 | \Psi_7' \rangle - \mathfrak{M}_{rel} \ . \tag{42}$$

In the evaluation of all the perturbing terms we use the nonrelativistic form (31). We find

$$\begin{aligned} \mathfrak{M}_{II} &= [(\alpha_7 c_6 + \beta_7 d_6)(\alpha_6 a_6 + \beta_6 b_6) \\ &\quad + (\alpha_7 c_7 + \beta_7 d_7)(\alpha_6 a_7 + \beta_6 b_7)] \\ &\quad \times \tfrac{1}{2}[g(^4P_{1/2}) - g(^2P_{1/2})] \times \tfrac{1}{2}e \\ &= -1.9 \times 10^{-6}\mu_B \ . \end{aligned} \tag{43}$$

Inclusion of higher s-state excitations ($6s\,ns\,np$) does not significantly change Eq. (43). However, since the electrostatic exchange integrals are fairly sensitive to small changes in wave functions, the fourth-order result (43) might be in error by as much as a factor of 2.

C. Breit interaction corrections

The OECF approximation used up to now does not include a complete description of electron-electron interactions, even if we assume a spherically symmetric core. To order v^2/c^2, the electron-electron interaction contributes a term to the Hamiltonian

$$\Delta H = \sum_{i<k} \frac{e^2}{r_{ik}} - \frac{e^2}{2}\sum_{i<k}\left(\frac{\vec{\alpha}_i \cdot \vec{\alpha}_k}{r_{ik}} + \frac{(\vec{\alpha}_i \cdot \vec{r}_{ik})(\vec{\alpha}_k \cdot \vec{r}_{ik})}{r_{ik}^3}\right). \tag{44}$$

The first term on the RHS of (44) is in fact partially included in the central potential [Eq. (4)], but the second term is not, and must be regarded as an additional perturbation. This term may be reduced to the following expression (Breit interaction)[15]

$$\Delta H_B = \frac{e^2}{2}\sum_{i\neq k}\left(\vec{\nabla}_i \frac{1}{r_{ik}}\times\vec{p}_i\right)\cdot\vec{\sigma}_k - \frac{e^2}{2}\sum_{i<k}\left(\frac{1}{r_{ik}}\vec{p}_i\cdot\vec{p}_k + \frac{1}{r_{ik}^3}(\vec{r}_{ik}\cdot(\vec{r}_{ik}\cdot\vec{p}_i)\cdot\vec{p}_k)\right). \quad (45)$$

In order to calculate the contribution of this interaction to the $M1$ transition, we replace $\vec{p}$ by $\vec{p}+e\vec{A}$ (electron charge $=-e$), where $\vec{A}=\frac{1}{2}(\vec{B}\times\vec{r})$. Thus we obtain

$$\Delta H_{B,\mathrm{eff}} = \frac{e^3}{2}\sum_{i\neq k}(\vec{\nabla}_i\frac{1}{r_{ik}}\times\vec{A}_i)\cdot\vec{\sigma}_k - \frac{e^3}{2}\sum_{i\neq k}\left(\frac{\vec{A}_i\cdot\vec{p}_k}{r_{ik}} + \frac{(\vec{r}_{ik}\cdot\vec{A}_i)(\vec{r}_{ik}\cdot\vec{p}_k)}{r_{ik}^3}\right). \quad (46)$$

This expression has been derived previously by Abragam and Van Vleck[16] and Schwartz.[17] We now consider the special case of one electron outside a spherically symmetric electron distribution; it has been shown that only electrons outside of closed shells give nonvanishing contributions.[16]

It can then be shown that the matrix element of the first term on the RHS of (46), called the Lamb correction,[18] is

$$\mathfrak{M}_L = \frac{-e^3}{2}\int\psi_1'^*(\vec{r}_1)\vec{\sigma}_1\cdot\vec{\nabla}_1\times\left(\int\frac{\vec{A}(r_2)\rho(\vec{r}_2)\,d\tau_2}{|\vec{r}_1-\vec{r}_2|}\right)\times\psi_1(\vec{r}_1)\,d\tau_1\,, \quad (47)$$

where

$$\rho(\vec{r}_2)=\sum_{k\neq 1}\psi_k^*(\vec{r}_2)\psi_k(\vec{r}_2)\,.$$

For present purposes we choose ψ_1, ψ_1' to be $6P_{1/2}$, $7P_{1/2}$ wave functions, respectively; for $\rho(\vec{r}_2)$ we insert the spherically symmetric density obtained from our central potential, and we set $\vec{B}\|z$. Then the amplitude for the $m_J=\frac{1}{2}\to m_{J'}=\frac{1}{2}$ transition is reduced to a sum of radial integrals:

$$\mathfrak{M}_L=\tfrac{1}{2}eB(-\tfrac{4}{45}e^2\langle V\rangle+\tfrac{1}{9}e^2\langle W\rangle)\,, \quad (48)$$

where

$$\langle V\rangle=\int_0^\infty\frac{F(r_1)}{r_1^3}\left(\int_0^{r_1}r_2^4\rho(r_2)\,dr_2\right)F'(r_1)r_1^2\,dr_1\,, \quad (49)$$

$$\langle W\rangle=\int_0^\infty F(r_1)\left(\int_{r_1}^\infty\rho(r_2)r_2\,dr_2\right)F'(r_1)r_1^2\,dr_1\,, \quad (50)$$

and F, F' are the nonrelativistic $6p$, $7p$ radial wave functions, respectively. The resulting contribution to $\mathfrak{M}$ is evaluated numerically to be

$$\mathfrak{M}_L=-4\times10^{-7}\mu_B\,. \quad (51)$$

The second term on the RHS of (46), called the orbit-orbit correction,[16] gives the following matrix element:

$$\mathfrak{M}_{\mathrm{OR}}=\frac{-e^3}{6}\int\psi_1^*(\vec{r}_1)\left(\frac{1}{r_1^3}\int_0^{r_1}\rho(r_2)r_2^4\,dr_2+\int_{r_1}^\infty\rho(r_2)r_2\,dr_2\right)\times\vec{L}_1\cdot\vec{B}\psi_1'(\vec{r}_1)\,d^3r_1\,. \quad (52)$$

For $\vec{B}\|\hat{z}$, $m_J=\frac{1}{2}\to m_J'=\frac{1}{2}$, this becomes

$$\mathfrak{M}_{\mathrm{OR}}=-\tfrac{1}{9}e^3B(\langle W\rangle+\langle V\rangle)\,, \quad (53)$$

which yields the following numerical contribution to $\mathfrak{M}$:

$$\mathfrak{M}_{\mathrm{OR}}=-1.20\times10^{-5}\mu_B\,. \quad (54)$$

D. Total theoretical $M1$ rate; corrections to $g_J(\mathrm{Tl}, 6^2P_{1/2})$

We collect the four contributions to the $M1$ amplitude [Eqs. (32), (43), (51), and (54)]:

$$\mathfrak{M}=\mathfrak{M}_{\mathrm{REL}}+\mathfrak{M}_{II}+\mathfrak{M}_L+\mathfrak{M}_{\mathrm{OR}}=-3.2\times10^{-5}\mu_B\,. \quad (55)$$

Our analysis of hyperfine structure indicates that there is an uncertainty of ~20% in the calculation of relativistic effects. In addition, $\mathfrak{M}_{II}$ has an independent uncertainty of $\sim0.15\mathfrak{M}$. The combined theoretical uncertainty of $\mathfrak{M}$ [Eq. (55)] is estimated to be $\sim1.0\times10^{-5}\mu_B$.

The Zeeman energy shift in a constant magnetic field B is related to g_J by

$$\Delta E=\mu_B g_J m_J B\,. \quad (56)$$

In zeroth order

$$g_J=\frac{J(J+1)+L(L+1)-S(S+1)}{2J(J+1)}+g_S\frac{J(J+1)+S(S+1)-L(L+1)}{2J(J+1)}\,,$$

where $g_S=2.002\,319\,114$. The corrections to g_J are obtained in the same manner as those described in Secs. III A–III C, merely by computing $6^2P_{1/2}$

TABLE V. g-factor anomaly calculation and comparison with experiment.

Measured $6^2P_{1/2}$ g factor	0.665 692 4(18) [a]
Zero-order theory	0.665 893 6
g-factor anomaly	−0.000 201 2(18) [a]
Calculated anomaly	
Relativistic	−0.000 107
Configuration interaction	< 0.000 001
Lamb	−0.000 006
Orbit-orbit	−0.000 082
Total calculated anomaly	−0.000 195

[a] Reference 19.

$-6^2P_{1/2}$ diagonal matrix elements. The results of this calculation are displayed in Table V and compared with experiment.[19] The agreement is very good.

E. Hyperfine mixing

Next, we calculate the additional contributions to the $M1$ amplitude arising from admixture to $6P$, $7P$ wave functions of $7P$, $6P$ components, respectively, due to hyperfine interaction. According to first-order perturbation theory,

$$|\overline{6^2P}_{1/2}, F\rangle = |6^2P_{1/2}, F\rangle + \frac{\langle 7^2P_{1/2}, F|H_{\rm hfs}|6^2P_{1/2}, F\rangle}{E_{6p}-E_{7p}} \times |7^2P_{1/2}, F\rangle \ , \quad (57)$$

$$|\overline{7}^2\overline{P}_{1/2}, F'\rangle = |7^2P_{1/2}, F'\rangle + \frac{\langle 6^2P_{1/2}, F'|H_{\rm hfs}|7^2P_{1/2}, F'\rangle}{E_{7p}-E_{6p}} \times |6^2P_{1/2}, F'\rangle \ , \quad (58)$$

where the $|\bar{}\rangle$ indicates a perturbed state, and $H_{\rm hfs}$, given by Eq. (16), is diagonal in F, the total atomic angular momentum. This contributes to the $M1$ transition matrix element as follows:

$$\langle \overline{7}^2\overline{P}_{1/2}, F'|M1|\overline{6}^2\overline{P}_{1/2}, F\rangle_{\rm hfs} \cong (\langle 7P, F|H_{\rm hfs}|6P, F\rangle - \langle 6P, F'|H_{\rm hfs}|7P, F'\rangle) \times \frac{1}{E_{6p}-E_{7p}} \langle nP_{1/2}, F'|M1|nP_{1/2}, F\rangle \ , \quad (59)$$

where on the RHS we use the nonrelativistic $M1$ operator, whose matrix elements are independent of principal quantum number n. It is interesting to note that the LHS of Eq. (59) vanishes for $F=F'$; thus this correction, unlike the previous ones, only affects $F=0\to F'=1$ and $F=1\to F'=0$ transitions. The hyperfine matrix elements on the RHS may be computed by the methods of Sec. II C with the following results:

For $F=0$, $F'=1$,

$$\langle M1\rangle_{\rm hfs}^{F'=1,F=0} = +2.6\times10^{-6}\mu_B \ . \quad (60)$$

For $F=1$, $F'=0$,

$$\langle M1\rangle_{\rm hfs}^{F'=0,F=1} = -2.6\times10^{-6}\mu_B \ . \quad (61)$$

F. Other $M1$ transitions

The methods outlined in Secs. III A–III C and III E may be used to calculate other Tl $M1$ transitions, forbidden or allowed. These include the $6^2P_{1/2}$-$6^2P_{3/2}$ transition (allowed) which has been suggested as an interesting candidate for a neutral current experiment, and the $6^2P_{1/2}$-$7^2P_{3/2}$, $6^2P_{3/2}$-$7^2P_{1/2}$ transitions which are not so strongly forbidden as $nP_{1/2}$-$n'P_{1/2}$ and $nP_{3/2}$-$n'P_{3/2}$ cases, since for $\frac{1}{2}\nleftrightarrow\frac{3}{2}$ the radial wave functions are not fully orthogonal. In what follows we ignore the small higher-order effects considered in Secs. III B, III C, and III E and consider only the one-electron amplitude of Eq. (28). For $nP_{3/2}$-$nP_{1/2}$ transitions we find

$$A_{3/2\to1/2} = 2\pi\langle|V_{fi}|\rangle^2 = e^2\omega^3\left|\int\frac{g_1(kr)}{\omega}(f_{3/2}g_{1/2}+g_{3/2}f_{1/2})\right|^2 \quad (62)$$

and similarly for $\frac{1}{2}\to\frac{3}{2}$ transitions. The results are tabulated in Table VI. In the allowed cases, the $M1$ matrix elements are within 2% of the nonrelativistic value $-\sqrt{2}/3$, while the forbidden ($6^2P_{1/2}$-$7^2P_{3/2}$, $6^2P_{3/2}$-$7^2P_{1/2}$) matrix elements are about 10% of the allowed values, which corresponds to the expected magnitude of spin-orbit coupling effects.

These transitions also have nonzero electric quadrupole ($E2$) amplitudes. We obtain

$$A_{E2} \cong \tfrac{1}{75}e^2\omega^5\left(\int_0^\infty f_f r^2 f_i\,dr\right)^2 \quad (63)$$

since the portion of the $E2$ amplitude which is proportional to $\int g_f r^2 g_i\,dr$ is quite negligible. Table VI includes a tabulation of the $E2$ radial integrals and resulting A coefficients. The coefficient $A_{E2}(6^2P_{3/2}\to6^2P_{1/2})$ has also been calculated by

TABLE VI. $P_{1/2}$-$P_{3/2}$ $M1$ and $E2$ transition rates.

Transition	$\mathfrak{M}\times3/\sqrt{2}$	$A_{\mathfrak{M}1}$ (sec^{-1})	$\int_0^\infty f_f r^2 f_i\,dr$ (Å^2)	A_{E2} (sec^{-1})
$6^2P_{1/2}$-$6^2P_{3/2}$	+0.9796	4.083	2.94×10^5	0.158
$6^2P_{1/2}$-$7^2P_{3/2}$	−0.0902	3.31	-1.27×10^5	55.2
$7^2P_{1/2}$-$6^2P_{3/2}$	−0.115	2.18	-3.00×10^5	72.8
$7^2P_{1/2}$-$7^2P_{3/2}$	+0.9822	8.706×10^{-3}	2.40×10^6	3.69×10^{-4}

Garstang[20] and his result (0.11 $\sec^{-1}$) and ours are in agreement.

IV. PARITY-NONCONSERVING $E1$ AMPLITUDES

A. $6\,^2P_{1/2} \to 7\,^2P_{1/2}$ transition

As previously discussed (Sec. I) parity nonconservation in the electron-nucleon weak neutral interaction manifests itself in the matrix element

$$\langle \psi_1 | H_{\rm PN} | \psi_2 \rangle = (-GQ_W/2\sqrt{2})\,\psi_1^*(\vec{x})\gamma_5\psi_2(\vec{x})|_{x=0}\,. \quad (64)$$

We write the perturbed $6P$, $7P$ states as

$$|\bar{6}\bar{P}_{1/2}\rangle = |6P_{1/2}\rangle + \sum_n \frac{\langle nS_{1/2}|H_{\rm PN}|6P_{1/2}\rangle}{E_{6P}-E_{nS}}\,|nS_{1/2}\rangle\,, \quad (65)$$

$$|\bar{7}\bar{P}_{1/2}\rangle = |7P_{1/2}\rangle + \sum_n \frac{\langle nS_{1/2}|H_{\rm PN}|7P_{1/2}\rangle}{E_{7P}-E_{nS}}\,|nS_{1/2}\rangle\,. \quad (66)$$

From (64) we obtain

$$\langle nS_{1/2}|H_{\rm PN}|n'P_{1/2}\rangle = \frac{i}{4\pi}\frac{G}{2}\frac{Q_w}{\sqrt{2}}\frac{1}{r^2} \times [f_{ns}(r)g_{n'p}(r) - f_{n'p}(r)g_{ns}(r)]_{r=0}\delta_{m_s m_p}\,. \quad (67)$$

This expression is averaged over the nucleus assuming a constant proton and neutron density. As an alternative, one may assume a pointlike nucleus, and evaluate $\langle nS|H_{\rm PN}|n'P\rangle$ at the nuclear radius; this increases the numerical value by 6%. The $E1$ matrix element is obtained by evaluating

$$\langle \bar{7}\bar{P}_{1/2}|E1|\bar{6}\bar{P}_{1/2}\rangle = \sum_{ns}\frac{\langle 7P_{1/2}|E1|nS\rangle\langle nS|H_{\rm PN}|6P_{1/2}\rangle}{E_{6P}-E_{nS}} + \sum_{ns}\frac{\langle 7P_{1/2}|H_{\rm PN}|nS\rangle\langle nS|E1|6P_{1/2}\rangle}{E_{7P}-E_{nS}} \quad (68)$$

For the $E1$ matrix elements of the RHS of Eq. (68) we have

$$\langle nS|E1|P_{1/2}\rangle = e\langle nS|\hat{\epsilon}\cdot r|P_{1/2}\rangle = e\int f_S r f_p\,dr\cdot\chi_{-1}^{m_s}\hat{\epsilon}\cdot\tilde{e}_r\chi_1^{m_p} = \frac{e}{3}\int f_S r f_p\,dr, \quad (m_s = m_p = -\tfrac{1}{2}) \quad (69)$$

Expression (68) is evaluated by two methods:

(1) A sum is taken over the lowest five states $|6s^2ns\rangle$, $n>6$, and the effect of the autoionizing $|6s\,6p\,7p\rangle$ state is also taken into account by including in the sum a term corresponding to the unphysical state $|6s^26s\rangle$. (See Appendix B for this argument.)

(2) The operators

$$\sum_n \frac{|nS\rangle\langle nS|}{E_{n'P}-E_{nS}}$$

are replaced by Dirac Green's functions, described in detail in Appendix C. This calculation includes the contribution of all intermediate S states including continuum and autoionizing states and is thus more reliable and complete than method (1).

The results are summarized in Table VII. The Green's-function method yields the numerical value for $\epsilon_{\rm PN} = \langle \bar{7}\bar{P}_{1/2}|E1|\bar{6}\bar{P}_{1/2}\rangle$ in the Eq. (68)

TABLE VII. Calculation of $\mathcal{E}_{\rm PN}$.

Intermediate s state	Contributions to $\mathcal{E}_{\rm PN}$: $\frac{\langle 7P_{1/2}\|E1\|ns\rangle\langle ns\|H_{\rm PN}\|6P_{1/2}\rangle}{E_6-E_n}$	$\frac{\langle 7P_{1/2}\|H_{\rm PN}\|ns\rangle\langle ns\|E1\|6P_{1/2}\rangle}{E_7-E_n}$
	Method 1	
$\|6s\rangle$	$-i\,0.197\times10^{-10}Q_W\|\mu_B\|$	$+i\,0.631\times10^{-10}Q_W\|\mu_B\|$
$\|7s\rangle$	$+i\,5.08$	$-i\,1.69$
$\|8s\rangle$	$-i\,1.77$	$+i\,0.485$
$\|9s\rangle$	$-i\,0.232$	$+i\,0.093$
$\|10s\rangle$	$-i\,0.084$	$+i\,0.037$
Subtotals	$i\,2.81\times10^{-10}Q_W\|\mu_B\|$	$-i\,0.45\times10^{-10}Q_W\|\mu_B\|$
Total	$i\,2.36\times10^{-10}Q_W\|\mu_B\|$	
	Method 2	
	$i\,2.13\times10^{-10}Q_W\|\mu_B\|$	$-i\,0.20\times10^{-10}Q_W\|\mu_B\|$
Total	$i\,1.93\times10^{-10}Q_W\|\mu_B\|$	

TABLE VIII. $\mathcal{E}_{PN}$ for $n'P_{1/2}$-$nP_{3/2}$ transitions.

$$\sum \frac{e\langle nP_{3/2}|E1|ns\rangle\langle ns|H_{PN}|n'P_{1/2}\rangle}{E_{P_{1/2}}-E_s}$$

Intermediate s state	$6\,^2P_{3/2}$-$6\,^2P_{1/2}$	$7\,^2P_{3/2}$-$6\,^2P_{1/2}$	$6\,^2P_{3/2}$-$7\,^2P_{1/2}$
	Method 1		
$\|6s\rangle$	$-i\,4.22\times10^{-10}Q_W\|\mu_B\|$	$-i\,0.65$	$-i\,0.86$
$\|7s\rangle$	$-i\,2.83$	$+i\,6.76$	$+i\,3.43$
$\|8s\rangle$	$-i\,0.264$	$-i\,3.13$	$-i\,0.78$
$\|9s\rangle$	$-i\,0.084$	$-i\,0.30$	$-i\,0.14$
$\|10s\rangle$	$-i\,0.041$	$-i\,0.10$	$-i\,0.06$
Total	$-i\,7.45\times10^{-10}Q_W\|\mu_B\|$	$+i\,2.58\times10^{-10}Q_W\|\mu_B\|$	$+i\,1.58\times10^{-10}Q_W\|\mu_B\|$
	Method 2		
	$-i\,8.09\times10^{-10}Q_W\|\mu_B\|$	$+i\,1.75\times10^{-10}Q_W\|\mu_B\|$	$+i\,1.25\times10^{-10}Q_W\|\mu_B\|$

$$\mathcal{E}_{PN}=1.93i\times10^{-10}Q_W|\mu_B|, \tag{70}$$

which corresponds to an A coefficient:

$$A=1.20\times10^{-16}Q_W^2\ \text{sec}^{-1}. \tag{71}$$

In the Weinberg model,

$$Q_W=Z(1-4\sin^2\theta_W)-N\cong-140 \tag{72}$$

for Tl, using $\sin^2\theta_W=0.3$ as suggested by the experiment of Reines *et al.*[21] Thus we obtain from (70) and (72),

$$\mathcal{E}_{PN}=-2.70i\times10^{-8}|\mu_B|. \tag{73}$$

For the circular dichroism δ it can be shown that one obtains

$$\delta=\frac{2\text{Im}(\mathcal{E}_{PN})\mathfrak{M}}{|\mathfrak{M}|^2+|\epsilon|^2}\approx\frac{2\text{Im}(\mathcal{E}_{PN})}{\mathfrak{M}}. \tag{74}$$

Inserting (73) and the experimental value of $\mathfrak{M}$ from Eq. (3) in (74) we obtain

$$\delta=+2.6\times10^{-3}. \tag{75}$$

This result is to be compared with the original estimate of Bouchiat and Bouchiat,[4] $\delta\cong2\times10^{-3}$. Our result is also to be compared with the calculation of Sushkov, Flambaum, and Khriplovich,[22] who obtain, also using $\mathfrak{M}_{expt}$ from Eq. (3),

$$\delta=2.5\times10^{-3}. \tag{76}$$

B. Other parity-nonconserving transitions

For $P_{1/2}$-$P_{3/2}$ transitions we may ignore the effect of H_{PN} on the $P_{3/2}$ state since $J=\frac{3}{2}$ wave functions have extremely small amplitudes at the nucleus. Thus,

$$\langle\overline{P}_{3/2}|E1|\overline{P}_{1/2}\rangle=\sum_{nS}\frac{\langle P_{3/2}|E1|nS\rangle\langle nS|H_{PN}|P_{1/2}\rangle}{E_{P_{1/2}}-E_{nS}}. \tag{77}$$

These matrix elements were evaluated in the same way as described above for $\mathcal{E}_{PN}$. The results are summarized in Table VIII, where

$$\langle P_{3/2}|E1|nS\rangle=\frac{e\sqrt{2}}{3}\int_0^\infty f_{P_{3/2}}rf_{S_{1/2}}dr. \tag{77a}$$

V. STARK EFFECT

A. $6\,^2P_{1/2}$-$7\,^2P_{1/2}$ transitons

We now calculate the electric-field-induced $E1$ transitions which can occur between $6\,^2P_{1/2}$, $7\,^2P_{1/2}$ levels through Stark-mixing with $^2S_{1/2}$, $^2D_{3/2}$ states. The coordinate system is shown in Fig. 2. Action of the perturbation $H'=e\vec{E}\cdot\vec{r}=eE_0y$ results in the perturbed states

$$|\overline{NP}_{1/2}\rangle=|NP_{1/2}\rangle+\sum_{nS}\frac{|nS\rangle\langle nS|eE_0y|NP_{1/2}\rangle}{E_{NP_{1/2}}-E_{nS}}+\sum_{nD_{3/2}}\frac{|nD_{3/2}\rangle\langle nD_{3/2}|eE_0y|NP_{1/2}\rangle}{E_{NP_{1/2}}-E_{nD_{3/2}}}. \tag{78}$$

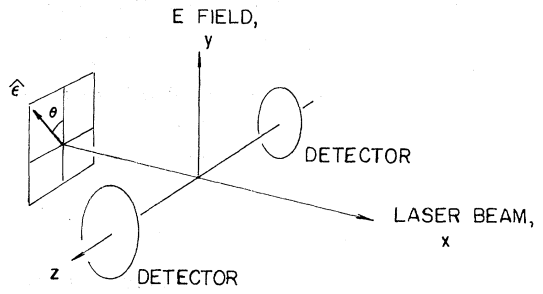

FIG. 2. Coordinate system and orientation of electric field $\vec{E}$, laser beam, and detectors as described in this paper and utilized in the experiment of Chu, Commins, and Conti.

Thus an electric dipole transition stimulated by laser photons with linear polarization

$$\hat{\epsilon} = \cos\theta\,\hat{y} + \sin\theta\,\hat{z} \tag{79}$$

has amplitude

$$\mathcal{E}_s = \langle \overline{7}^2\overline{P}_{1/2} | E1 | \overline{6}^2\overline{P}_{1/2} \rangle_{\text{Stark}}$$
$$= \sum_n \frac{\langle 7^2P_{1/2} | e\hat{\epsilon}\cdot\vec{r} | n\rangle\langle n | eE_0 y | 6^2P_{1/2}\rangle}{E_{6P_{1/2}} - E_n}$$
$$+ \sum_n \frac{\langle 7^2P_{1/2} | eE_0 y | n\rangle\langle n | e\hat{\epsilon}\cdot r | 6^2P_{1/2}\rangle}{E_{7P_{1/2}} - E_n}$$
$$\text{for } n = S_{1/2}, D_{3/2} \text{ states}. \tag{80}$$

The result of a calculation of this amplitude may be represented by a 2×2 matrix whose rows and columns are labeled by $m_J(6^2P_{1/2})$ and $m_J(7^2P_{1/2})$, respectively,

$$\mathcal{E}s = e^2E_0 \times$$

$m_J(7^2P_{1/2})$	$\frac{1}{2}$	$-\frac{1}{2}$ $= m_J(6^2P_{1/2})$
$=\frac{1}{2}$	$\alpha\cos\theta$	$-i\beta\sin\theta$
$=-\frac{1}{2}$	$-i\beta\sin\theta$	$\alpha\cos\theta$

(81)

Here

$$\alpha = \frac{1}{9}\sum R_{7P,nS}R_{6P,nS}\left(\frac{1}{E_7 - E_{nS}} + \frac{1}{E_6 - E_{nS}}\right)$$
$$+ \frac{2}{9}\sum_{nD_{3/2}} R_{7P,nD}R_{6P,nD}\left(\frac{1}{E_7 - E_{nD}} + \frac{1}{E_6 - E_{nD}}\right) \tag{82}$$

and

$$\beta = \frac{1}{9}\sum_{nS} R_{7P,nS}R_{6P,nS}\left(\frac{1}{E_6 - E_{nS}} - \frac{1}{E_7 - E_{nS}}\right)$$
$$+ \frac{1}{9}\sum_{nD_{3/2}} R_{7P,nD}R_{6P,nD}\left(\frac{1}{E_7 - E_{nD}} - \frac{1}{E_6 - E_{nD}}\right) \tag{83}$$

where $E_6 = E(6^2P_{1/2})$, $E_7 = E(7^2P_{1/2})$, and $R_{7P,nS} = \langle 7^2P_{1/2} | r | n^2S_{1/2}\rangle$, etc. The quantities α and β have been evaluated by summing over the nearest S and D states, and also by use of the Green's function, Appendix C. The results are summarized in Table IX.

Chu, Commins, and Conti have measured β/α. Their result,[3]

$$[\beta/\alpha]_{\text{expt}} = 0.84, \tag{84}$$

is in good agreement with the Green's-function value of Table IX. This theoretical value $\beta/\alpha = 0.80$ was employed by them to determine the experimental value of $\mathfrak{M}$, as described below.

TABLE IX. Calculation of Stark matrix elements.

Quantity summed	Finite sum over five lowest energy levels ($7^2S_{1/2}$-$11^2S_{1/2}$, $6^2D_{3/2}$-$10^2D_{3/2}$)	Green's function method
$\frac{R_{7P,nS}R_{nS,6P}}{E_6 - E_{nS}}$	3.78×10^{10}	3.64×10^{10}
$\frac{R_{7P,nS}R_{nS,6P}}{E_7 - E_{nS}}$	-2.58×10^{11}	-2.71×10^{11}
$\frac{R_{7P,nD}R_{nD,6P}}{E_6 - E_{nD}}$	3.50×10^{10}	2.81×10^{10}
$\frac{R_{7P,nD}R_{nD,6P}}{E_7 - E_{nD}}$	8.00×10^{11}	7.01×10^{11}
$e^2\alpha$ [in units $\mu_B/(\text{V/cm})$]	2.43×10^{-5}	2.05×10^{-5}
$e^2\beta$	1.78×10^{-5}	1.64×10^{-5}
β/α	0.73	0.80

B. Experimental determination of $M1$ amplitude

A finite $7^2P_{1/2}$ final-state polarization can arise along the $\hat{z}$ axis of Fig. 1 through interference between $\mathfrak{M}$ and/or $\mathcal{E}_{PN}$ and $\mathcal{E}_S$. Interference between $\mathfrak{M}$ and $\mathcal{E}_S$ may then be utilized to measure $\mathfrak{M}$. Here the effects of $\mathcal{E}_{PN}$, which are in any case very small, are neglected. In an extension of this experiment now underway, interference between $\mathcal{E}_{PN}$ and $\mathcal{E}_S$ is utilized to determine $\mathcal{E}_{PN}$ itself.

In order to facilitate comparison with observations in which some of the hfs components of the $6^2P_{1/2}$-$7^2P_{1/2}$ transition are resolved, we replace the matrix of Eq. (81) by one whose rows and columns are labeled by F', $m_{F'}$ (for $7^2P_{1/2}$) and F, m_F (for $6^2P_{1/2}$), respectively. Including $\mathcal{E}_{PN}$, $\mathfrak{M}$, and $\mathcal{E}_S$, the total dipole amplitude D is given in Table X.

In the experimental determination of $\mathfrak{M}$, the $6^2P_{1/2}$ hfs splitting, but not that of $7^2P_{1/2}$, is resolved. Thus the $7^2P_{1/2}$ polarization is given by the formula

$$P(F)=\frac{\sum_{m_F,m'_F} m_{F'}\left|D^{F',m_{F'}}_{F,m_F}\right|^2}{\sum_{m_{F'},m_F}\left|D^{F',m_{F'}}_{F,m_F}\right|^2}. \tag{85}$$

Neglecting $|\mathfrak{M}|^2$ compared to $|\mathcal{E}_S|^2$ (which is justifiable for the rather large E fields employed), Eq. (84) becomes the following for the four indicated cases of interest:

(a) $F=1$; $F'=1$ $\quad \hat{\epsilon}\|\vec{E}\ (\theta=0)$ $\quad P\cong \frac{4}{3}\mathfrak{M}/\alpha$

(b) $F=0$; $F'=0$ $\quad \hat{\epsilon}\|\vec{E}\ (\theta=0)$ $\quad P=0$

(c) $F=1$; $F'=1,0$ $\quad \hat{\epsilon}\perp\vec{E}\ (\theta=90°)$

$P=-\frac{2}{3}\mathfrak{M}/\beta$ ($7^2P_{1/2}$ hfs unresolved)

(d) $F=0$; $F'=1$ $\quad \hat{\epsilon}\perp\vec{E}\ (\theta=90°)$ $\quad P=-2\mathfrak{M}/\beta$.

We now apply the hfs mixing correction of Eq. (60) to case (d) [it also applies to case (c) but this was not observed in detail]. The resulting ratio $P_d^{\rm corr}/P_a$ is then in good agreement with experiment. From their measurements of P_a and/or P_d Chu *et al.*[3] obtain the experimental value of $\mathfrak{M}$ given in Eq. (3).

C. Interference of $\mathcal{E}_{PN}$ and $\mathcal{E}_S$

When the incident light is circularly polarized, it becomes possible to measure the interference between $\mathcal{E}_{PN}$ and $\mathcal{E}_S$, again by detecting the polarization of the $7^2P_{1/2}$ state (by means of circular polarization of its decay fluorescence). The formulas analogous to Eq. (85) are readily obtained from Table X. We quote only the result for the $F=0\to F'=1$ transition

$$P=\frac{\frac{1}{2}(\beta-f)^2-\frac{1}{2}(\beta+f)^2}{\frac{1}{2}(\beta+f)^2+\frac{1}{2}(\beta-f)^2+f^2}\approx\frac{-2f}{\beta}, \tag{86}$$

where $f=\mathfrak{M}-\eta\mathcal{E}_{PN}$, $\eta=\pm1$ for right-hand circular (left-hand circular) laser light, and the approximation $P\approx-2f/\beta$ is valid for large electric fields ($E\gg1$ V/cm).

VI. PARITY NONCONSERVATION IN $^2P_{1/2}$-$^2P_{3/2}$ TRANSITIONS

For the transitions $6^2P_{1/2}$-$6^2P_{3/2}$, $6^2P_{1/2}$-$7^2P_{3/2}$, and $6^2P_{3/2}$-$7^2P_{1/2}$, we include $E2$ as well as $M1$ contributions and write

$$\langle T\rangle=\langle P_{3/2}|\vec{\mu}\cdot\hat{x}\times\hat{\epsilon}+e\hat{\epsilon}\cdot\vec{r}+ie(\hat{\epsilon}\cdot\vec{r})(\vec{k}\cdot\vec{r})|P_{1/2}\rangle, \tag{87}$$

where $\vec{\mu}=(e\hbar/2mc)(\vec{L}+\vec{S})$, and $\hat{\epsilon}=\hat{y}\cos\theta+\hat{z}\sin\theta$. The resulting transition matrix is given in Table XI. The circular dichroism is calculated as in

TABLE X. Dipole transition amplitudes $D=\langle M1\rangle+\langle E1_{PN}\rangle+\langle E1_{Stark}\rangle$ for $6^2P_{1/2}$ $(F,m_F)\to 7^2P_{1/2}$ $(F',m_{F'})$ transitions. $\alpha'=e^2E_0\alpha$. $\beta'=e^2E_0\beta$.

$7^2P_{1/2}$ F'	$m_{F'}$ \ $6^2P_{1/2}$, F	0	1	1	1
	m_F	0	−1	0	1
0	0	$\alpha'\cos\theta$	$(i/\sqrt{2})(\mathfrak{M}\sin\theta-\beta'\sin\theta+\mathcal{E}_{PN}\cos\theta)$	$-\mathfrak{M}\cos\theta+\mathcal{E}_{PN}\sin\theta$	$(i/\sqrt{2})(\mathfrak{M}\sin\theta+\beta'\sin\theta+\mathcal{E}_{PN}\cos\theta)$
1	−1	$(i/\sqrt{2})(\mathfrak{M}\sin\theta-\beta'\sin\theta-\mathcal{E}_{PN}\cos\theta)$	$\alpha'\cos\theta-\mathfrak{M}\cos\theta+\mathcal{E}_{PN}\sin\theta$	$(-i/\sqrt{2})(\mathfrak{M}\sin\theta+\beta'\sin\theta+\mathcal{E}_{PN}\cos\theta)$	0
1	0	$-\mathfrak{M}\cos\theta$	$(i/\sqrt{2})(\mathfrak{M}\sin\theta-\beta'\sin\theta+\mathcal{E}_{PN}\cos\theta)$	$\alpha'\cos\theta$	$(-i/\sqrt{2})(\mathfrak{M}\sin\theta+\beta'\sin\theta+\mathcal{E}_{PN}\cos\theta)$
1	1	$(i/\sqrt{2})(-\mathfrak{M}\sin\theta+\beta'\sin\theta-\mathcal{E}_{PN}\cos\theta)$	0	$(i/\sqrt{2})(\mathfrak{M}\sin\theta-\beta'\sin\theta+\mathcal{E}_{PN}\cos\theta)$	$\alpha'\cos\theta+\mathfrak{M}\cos\theta-\mathcal{E}_{PN}\sin\theta$

TABLE XI. $P_{3/2}$-$P_{1/2}$ transition amplitudes.

$m_{P_{3/2}}$ \ $m_{P_{1/2}}$	$\frac{1}{2}$	$-\frac{1}{2}$
$\frac{3}{2}$	$\left(\frac{\sqrt{3}}{2}\mathfrak{M}+\frac{\mathcal{E}_2}{\sqrt{6}}\right)i\sin\theta$ $+i\frac{1}{2}\sqrt{3}\,\mathcal{E}_{PN}\cos\theta$	$-(\frac{2}{3})^{1/2}\mathcal{E}_2\cos\theta$
$\frac{1}{2}$	$-\mathfrak{M}\cos\theta+\mathcal{E}_{PN}\sin\theta$	$\left(\frac{\mathfrak{M}}{2}-\frac{\mathcal{E}_2}{\sqrt{2}}\right)i\sin\theta$ $+i\frac{1}{2}\mathcal{E}_{PN}\cos\theta$
$-\frac{1}{2}$	$\left(\frac{\mathfrak{M}}{2}-\frac{\mathcal{E}_2}{\sqrt{2}}\right)i\sin\theta$ $+\frac{1}{2}i\mathcal{E}_{PN}\cos\theta$	$-\mathfrak{M}\cos\theta+\mathcal{E}_{PN}\sin\theta$
$\frac{3}{2}$	$-(\frac{2}{3})^{1/2}\mathcal{E}_2\cos\theta$	$\left(\frac{\sqrt{3}}{2}\mathfrak{M}+\frac{\mathcal{E}_2}{\sqrt{6}}\right)i\sin\theta$ $+i\frac{1}{2}\sqrt{3}\,\mathcal{E}_{PN}\cos\theta$

Eq. (75) with the result

$$\delta=\frac{2\mathfrak{M}\cdot\mathrm{Im}(\mathcal{E}_{PN})}{|\mathfrak{M}|^2+\frac{2}{3}|\langle\mathcal{E}_2\rangle|^2}. \tag{88}$$

The numerical results are summarized in Table XII.

The transition $6\,^2P_{1/2}$-$6\,^2P_{3/2}$ has been discussed as a candidate for optical rotation experiments to detect parity nonconservation. We compare our value of $\delta(6\,^2P_{1/2}\text{-}6\,^2P_{3/2})=4.17\times10^{-7}$, with that obtained from the calculation of Henley and Wilets,[23]

$$\delta=4.80\times10^{-7},\quad \text{for } \sin^2\theta_W=0.3. \tag{89}$$

The discrepancy of 15% is largely due to the $\langle\mathcal{E}_2\rangle$ amplitude which Henley and Wilets ignored. Once this correction is made, the two calculations agree within 2%. Henley and Wilets used a Green's-function technique with hybrid Dirac-Schrödinger wave functions; that is, relativistic wave functions are calculated for very small r and matched to nonrelativistic functions at larger r. Empirical energies rather than calculated energies (which in their case differ by ~20%) are inserted, although it is claimed that this does not change $\mathcal{E}_{PN}$ substantially. Since Henley and Wilets do not report calculations of Tl parameters other than $\mathcal{E}_{PN}$ $(6\,^2P_{1/2}\text{-}6\,^2P_{3/2})$ we cannot make an accurate comparison of their calculation with ours or with experiments.

We note in passing that in calculations[23,24] of the optical rotation of the currently investigated $^4S_{3/2}$-$^2D_{3/2}$ and $^4S_{3/2}$-$^2D_{5/2}$ transitions in bismuth, the effect of $\langle\mathcal{E}_2\rangle$ is ignored. In the calculations of Garstang[20] for these transitions, the $\mathcal{E}_2$ amplitude in $^4S_{3/2}$-$^2D_{3/2}$ is in fact negligible, but the large $\mathcal{E}_2$ amplitude calculated for $^4S_{3/2}$-$^2D_{5/2}$ would reduce the optical rotation by ~30%. A more precise calculation may alter this result substantially.

The Tl transitions $6\,^2P_{3/2}$-$7\,^2P_{1/2}$, $6\,^2P_{1/2}$-$7\,^2P_{3/2}$ may also be considered in optical rotation experiments, although the experimental difficulties are formidable.

ACKNOWLEDGMENTS

We thank Professor C. Schwartz, Dr. Peter Mohr, and Dr. Steven Chu for numerous useful discussions.

APPENDIX A: INTERCONFIGURATION INTERACTION AND HYPERFINE STRUCTURE OF THE $6\,^2P_{3/2}$ STATE

It is well known that the observed hfs of the $6\,^2P_{3/2}$ state in Tl differs markedly from that calculated in the OECF approximation using the single $5d^{10}6s^2 6p_{3/2}$ configuration, because the actual atomic state contains admixtures of other configu-

TABLE XII. Amplitudes for $P_{3/2}$-$P_{1/2}$ transitions.

Transition amplitude	$6P_{3/2}$-$6P_{1/2}$	$7P_{3/2}$-$7P_{1/2}$	$6P_{3/2}$-$7P_{1/2}$
$\mathfrak{M}$	$0.98\sqrt{2}/3$	$-0.092\sqrt{2}/3$	$-0.115\sqrt{2}/3$
$\mathcal{E}_2$	0.22	−0.434	0.767
$\mathcal{E}_{PN}$	$-i\,8.09\times10^{-10}Q_W$	$+i\,1.75\times10^{-10}Q_W$	$+i\,1.26\times10^{-10}Q_W$
$\delta(Q_W=-140)$	4.17×10^{-7}	1.67×10^{-8}	4.85×10^{-9}

$$\mathfrak{M}=\frac{-\sqrt{2}}{\omega}\int(f_{1/2}g_{3/2}+g_{1/2}f_{3/2})g_1(\omega r)\,dr\ \ |\mu_B|,$$

$$\mathcal{E}_2=\frac{2\omega}{5}\int f_{1/2}f_{3/2}r^2\,dr\ \ |\mu_B|,$$

$$\mathcal{E}_{PN}=\frac{2\sqrt{2}}{3}\sum\frac{\langle P_{3/2}|r|ns\rangle\langle ns|H_{PN}|P_{1/2}\rangle}{E_{1/2}-E_n}\ \ |\mu_B|.$$

TABLE XIII. Configuration interaction contributions to Hfs.

State	Unperturbed hfs splitting: ΔE_0 (GHz)	hfs splitting including $(6s7s6p)$ correction: $\Delta E_1 = \Delta E_0 + \delta(6s7s6p)$	$\Delta E_2 = \Delta E_1 + \delta(6s8s6p) + \delta(6s9s6p)$	Observed hfs splitting
$6^2P_{1/2}$	21.8	22.1	22.1	21.33
$6^2P_{3/2}$	3.27	1.37	0.81	0.528

rations,[25] notably $(\ldots 6s7s6p)$. We write the unperturbed wave function $(\ldots 6s^2 6p)$ as ψ_0 and form two possible $P_{3/2}$ (or $P_{1/2}$) states from the $6s7s6p$ configuration. These are $\psi_1(6s7s(^3S_1)6p\,^2P_J)$ with the $2s$ electrons in a spin-one state, and $\psi_2(6s7s(^1S_0)6p\,^2P_J)$ with the total s electron spin equal to zero. The states and notation are similar to those of Koster,[26] who performs a similar calculation for gallium. We write for the total wave function

$$\psi = \alpha_0\psi_0 + \alpha_1\psi_1 + \alpha_2\psi_2 . \tag{A1}$$

The coefficients α_1, α_2 are given in first-order perturbation theory by

$$\alpha_1 = \langle\psi_1|V|\psi_0\rangle/(E_0 - E_1) \tag{A2}$$

and

$$\alpha_2 = \langle\psi_2|V|\psi_0\rangle/(E_0 - E_2) , \tag{A3}$$

where $V = \sum_{i<j} e^2/r_{ij}$ and the matrix elements of V in (A2) and (A3) are calculated from the electrostatic integral

$$F_0(6s,6s;6s,7s) = \int\int \psi_{6s}(\vec{x}_1)\psi_{6s}(\vec{x}_2)\frac{e^2}{r_{12}} \times \psi_{6s}(\vec{x}_1)\psi_{7s}(\vec{x}_2)\,d\tau_1\,d\tau_2$$

and the similar direct and exchange integrals $F_0(6s,6p;7s,6p)$ and $G_1(6s,6p;6p,7s)$. We use the $6s$ wave function (ionization energy $= 2.3376 \times 10^{-5}$) calculated from Eq. (4). This is not self-consistent, since that central potential already includes the $6s^2$ charge distribution. However, this introduces an error estimated at only 10–15% in the ionization energy. The $7s$ and $6p_J$ states are calculated in the same central potential, and the energy denominator is approximated by the $6S$-$7S$ energy difference. Normalizing with $\alpha_0^2 + \alpha_1^2 + \alpha_2^2 = 1$, we find

$$\begin{aligned} &6P_{1/2}\text{:}\quad \alpha_0 = 0.97 \quad \alpha_1 = 0.0097 \quad \alpha_2 = 0.23 , \\ &6P_{3/2}\text{:}\quad \alpha_0 = 0.97 \quad \alpha_1 = 0.029 \quad \alpha_2 = 0.22 . \end{aligned} \tag{A4}$$

The large difference $\alpha_1(P_{3/2}) - \alpha_1(P_{1/2})$ occurs because of a corresponding difference in the exchange integral $G_1(6s,6p;6p,7s)$ between $6P_{3/2}$ and $6P_{1/2}$ states.

The hfs splitting is

$$\begin{aligned} \Delta_{3/2} &= \Delta_0(6^2P_{3/2}) + \tfrac{4}{9}\alpha_1^2(\Delta_{6s} + \Delta_{7s}) \\ &\quad - (4/3\sqrt{3})\alpha_1\alpha_2(\Delta_{6s} - \Delta_{7s}) \\ &\quad - (2/3\sqrt{6})\alpha_1\alpha_2(\Delta_{6s}\Delta_{7s})^{1/2} , \\ \Delta_{1/2} &= \Delta_0(6^2P_{1/2}) + \tfrac{2}{9}\alpha_1^2(\Delta_{6s} + \Delta_{7s}) \\ &\quad + (2/3\sqrt{3})\alpha_1\alpha_2(\Delta_{6s} - \Delta_{7s}) \\ &\quad + (4/3\sqrt{6})(\Delta_{6s}\Delta_{7s})^{1/2} , \end{aligned} \tag{A5}$$

where only the dominating s-electron perturbation is included. In formulas (A5) we use the experimental value of Δ_{7S}, Eq. (A4), and the calculated value $\Delta_{6S} = 135$ GHz. The numerical results are summarized in Table XIII. They show that the $6^2P_{3/2}$ hfs is strongly affected by configuration mixing while the $6^2P_{1/2}$ hfs is not. Further, similar corrections can be obtained for $6snsnp$ configurations with $n > 7$. That of the $6s8s6p$ and $6s9s6p$ configurations is also included in Table XIII. We find for $6s8s6p_{3/2}$, $\alpha_1 = 0.012$, $\alpha_2 = 0.09$; while for $6s9s6p_{3/2}$, $\alpha_1 = 0.007$, $\alpha_2 = 0.05$. Because of the uncertainties and lack of self-consistency inherent in the present approach, there is no profit in attempting to include contributions of configurations $6snsnp_{3/2}$ with $n > 9$.

APPENDIX B

We demonstrate that the effect of the $6s6p7p$ autoionizing state is taken into account (approximately) by calculating the amplitude $\mathcal{E}_{\rm PN}$ if a term corresponding to the unphysical $6s^2 6s$ state is included.[29] The term in question is

$$T = \frac{\langle 6s6s7p|\hat{\epsilon}\cdot r|6s6p7p\rangle\langle 6s6p7p|H'_{\rm PN}|6s6s6p\rangle}{E_{6s6s6p} - E_{6s6p7p}} + \frac{\langle 6s6s7p|H'_{\rm PN}|6s6p7p\rangle\langle 6s6p7p|\hat{\epsilon}\cdot r|6s6s6p\rangle}{E_{6s6s7p} - E_{6s6p7p}} . \tag{B1}$$

Now,

$$\langle 6s6s7p|\hat{\epsilon}\cdot\vec{r}|6s6p7p\rangle\langle 6s6p7p|H'|6s6s6p\rangle$$
$$=-\langle 6s|\hat{\epsilon}\cdot\vec{r}|6p\rangle\langle 7p|H'_{\rm PN}|6s\rangle$$
$$=-\langle 7p|H'_{\rm PN}|6s\rangle\langle 6s|\hat{\epsilon}\cdot\vec{r}|6p\rangle \quad \text{(B2)}$$

and

$$\langle 6s6s7p|H'_{\rm PN}|6s6p7p\rangle\langle 6s6p7p|\hat{\epsilon}\cdot\vec{r}|6s6s6p\rangle$$
$$=-\langle 7p|\hat{\epsilon}\cdot\vec{r}|6s\rangle\langle 6s|H'_{\rm PN}|6p\rangle . \quad \text{(B3)}$$

Furthermore,

$$E_{6s6s7p}-E_{6s6p7p}\cong -(E_{6p}-E_{6s}) \quad \text{(B4)}$$

and

$$E_{6s6s6p}-E_{6s6p7p}\cong -(E_{7p}-E_{6s}) . \quad \text{(B5)}$$

Inserting (B2)–(B5) in (B1) we obtain

$$T=\frac{\langle 7p|\hat{\epsilon}\cdot\vec{r}|6s\rangle\langle 6s|H'_{\rm PN}|6p\rangle}{E_{6p}-E_{6s}}+\frac{\langle 7p|H'_{\rm PN}|6s\rangle\langle 6s|\hat{\epsilon}\cdot\vec{r}|6p\rangle}{E_7-E_{6s}}, \quad \text{(B6)}$$

which is the desired result.

APPENDIX C: CONSTRUCTION AND USE OF THE DIRAC GREEN'S FUNCTION

The construction of the Dirac Green's function has been described by Mohr[27] and Gyulassy,[28] with emphasis on the case of a spherically symmetric central potential. This function is a solution of the differential equation:

$$[H(\vec{r}_2)-E]G(\vec{r}_1,\vec{r}_2,E)=I\delta^3(\vec{r}_2-\vec{r}_1) , \quad \text{(C1)}$$

where H is the Dirac Hamiltonian with potential $V(\vec{r}_2)=V(|\vec{r}_2|)$ and I is the 4×4 identity matrix. Separation of radial and angular variables is accomplished by writing

$$G(\vec{r}_2,\vec{r}_1,E)=\sum_{\kappa,\mu}\begin{pmatrix} G_\kappa^{11}(r_2,r_1,E)\chi_\kappa^\mu(\vec{e}_2)\chi_\kappa^{\mu\dagger}(\vec{e}_1) & -iG_\kappa^{12}(r_2,r_1,E)\chi_\kappa^\mu(\vec{e}_2)\chi_{-\kappa}^{\mu\dagger}(\vec{e}_1) \\ iG_\kappa^{21}(r_2,r_1,E)\chi_{-\kappa}^\mu(\vec{e}_2)\chi_\kappa^{\mu\dagger}(\vec{e}_1) & G_\kappa^{22}(r_2,r_1,E)\chi_{-\kappa}^\mu(e_2)\chi_{-\kappa}^{\mu\dagger}(\vec{e}_1)\end{pmatrix} , \quad \text{(C2)}$$

where the $\chi_\kappa(\vec{e})$ are the same functions as defined in Eq. (13). Eq. (C2) is justified by the completeness relation

$$\sum_{\kappa,\mu}\chi_\kappa^\mu(\vec{e}_2)\chi_\kappa^{\mu\dagger}(\vec{e}_1)=\begin{pmatrix}1&0\\0&1\end{pmatrix}\delta(\phi_2-\phi_1)\delta(\cos\theta_2-\cos\theta_1) .$$

Only $G_{\kappa=-1}^{ij}$ contributes to $\mathcal{E}_{\rm PN}$ ($S_{1/2}$ states) while for $\mathcal{E}_S$ (Stark mixing), the terms $G_{\kappa=-1}^{ij}$ ($S_{1/2}$ states) and $G_{\kappa=2}^{ij}$ ($D_{3/2}$ states) contribute. Eq. (C1) reduces to a 2×2 radial equation:

$$\begin{pmatrix} 1+V(r_2)-E & -\frac{1}{r_2}\frac{\partial}{\partial r_2}(r_2)+\frac{\kappa}{r_2} \\ \frac{1}{r_2}\frac{\partial}{\partial r_2}(r_2)+\frac{\kappa}{r_2} & -1+V(r_2)-E\end{pmatrix}\begin{pmatrix} G_\kappa^{11}(r_2,r_1,E) & G_\kappa^{12}(r_2,r_1,E) \\ G_\kappa^{21}(r_2,r_1,E) & G_\kappa^{22}(r_2,r_1,E)\end{pmatrix}=\begin{pmatrix}1&0\\0&1\end{pmatrix}\frac{\delta(r_2-r_1)}{r_2r_1} . \quad \text{(C3)}$$

It can be shown that the solution of (C3) is

$$G_\kappa(r_2,r_1,E)=\frac{1}{J^\kappa(E)}\left\{\theta(r_1-r_2)\begin{pmatrix}F_<^\kappa(r_2)F_>^\kappa(r_1) & F_<^\kappa(r_2)G_>^\kappa(r_1)\\ G_<^\kappa(r_2)F_>^\kappa(r_1) & G_<^\kappa(r_2)G_>^\kappa(r_1)\end{pmatrix}+\theta(r_2-r_1)\begin{pmatrix}F_>^\kappa(r_2)F_<^\kappa(r_1) & F_>^\kappa(r_2)G_<^\kappa(r_1)\\ G_>^\kappa(r_2)F_<^\kappa(r_1) & G_>^\kappa(r_2)G_<^\kappa(r_1)\end{pmatrix}\right\} , \quad \text{(C4)}$$

where $J^\kappa(E)=r^2\{G_<^\kappa(r)F_>^\kappa(r)-G_>^\kappa(r)F_<^\kappa(r)\}$ is the Wronskian and F^κ and G^κ are solutions of the equation

$$\begin{pmatrix} 1+V(r)-E & -\frac{1}{r}\frac{d(r)}{dr}+\frac{\kappa}{r} \\ \frac{1}{r}\frac{d(r)}{dr}+\frac{\kappa}{r} & -1+V(r)-E\end{pmatrix}\begin{pmatrix}F\\G\end{pmatrix}=0 . \quad \text{(C5)}$$

$\binom{F_<}{G_<}$ is the solution which is regular as $r\to 0$, while $\binom{F_>}{G_>}$ is the solution regular as $r\to\infty$. These solutions are calculated in the same manner as the eigensolutions of Eq. (11), that is, by numerical integration of the differential equation starting with the asymptotic solution either for small r [for $F_<, G_<$ and using $V(r)$ in (c) of Sec. IIA] or for large r [for $F_>, G_>$, using $V(r)\to -e^2/r$]. We note that F and G of (C5) correspond to f/r and g/r of Eq. (13).

The parity-nonconserving amplitude $\mathcal{E}_{\rm PN}$ of Eq. (68) can be written as

$$\mathcal{E}_{\rm PN} = -\int\int \langle \psi^{\mu_1}_{7^2P_{1/2}}(\vec{r}_1)\,|\,e\vec{\epsilon}\cdot\vec{r}G(\vec{r}_1,\vec{r}_2,E_{6p})H_{\rm PN}\,|\,\psi^{\mu_2}_{6^2P_{1/2}}(\vec{r}_2)\rangle\, d^3\vec{r}_2\, d^3\vec{r}_1$$
$$-\int\int \langle \psi^{\mu_1}_{7^2P_{1/2}}(\vec{r}_1)\,|\,H_{\rm PN}G(\vec{r}_1,\vec{r}_2,E_{7p})e\hat{\epsilon}\cdot\vec{r}\,|\,\psi^{\mu_2}_{6^2P_{1/2}}(\vec{r}_2)\rangle\, d^3\vec{r}_2\, d^3\vec{r}_1 . \tag{C6}$$

Because of the short-range character of $H_{\rm PN}$, the first term in (C6) becomes

$$-e\int_0^\infty f_{7p}r_2[r_2F_>^{(\kappa=-1)}(r_2,E_6)]\,dr_2\int \chi_1^{m_1\dagger}(\hat{\epsilon}\cdot\hat{e}_r)\chi_{-1}^{m_2}\frac{iGQ_W}{8\pi\sqrt{2}}\frac{1}{J(E_6)R^2}$$
$$\times\{[RF_<^{(\kappa=-1)}(R,E_6)]\,g_{6p}(R)-[RG_<^{(\kappa=-1)}(R,E_6)]f_{6p}(R)\},\quad R<r_{\rm nuc} \tag{C7}$$

In practice this expression is averaged over the region $R\le r_{\rm nuc}$, where $r_{\rm nuc}$ is the nuclear radius. The second term in (C6) becomes

$$+e\int f_{6p}r_1[r_1F_>^{(\kappa=-1)}(r_1,E_7)]\,dr_1\int \chi_{-1}^{m_1\dagger}\hat{\epsilon}\cdot\hat{e}_r\chi_1^{m_2}$$
$$\times\frac{iGQ_W}{8\pi\sqrt{2}}\frac{1}{J(E_7)R^2}\{[RF_<^{(\kappa=-1)}(R,E_7)]\,g_{7p}(R)-[RG_<^{(\kappa=-1)}(R,E_7)]\,f_7(R)\}. \tag{C8}$$

A similar calculation was performed for $\mathcal{E}_S$ (Sec. V). In this case only "large" components (f,F) contribute significantly. For example, the matrix element α of Eq. (82) is written

$$\alpha = -\frac{1}{9}\Big[\int_0^\infty\int_0^\infty \frac{f_{7p}(r_2)r_2[r_<F_<^{(\kappa=-1)}(r_<,E_6)]\,[r_>F_>^{(\kappa=-1)}(r_>,E_6)]\,r_1f_{6p}(r_1)\,dr_1\,dr_2}{J(E_6)}$$
$$+\int_0^\infty\int_0^\infty \frac{f_{7p}(r_2)r_2[r_<F_<^{(\kappa=-1)}(r_<E_7)]\,[r_>F_>^{(\kappa=-1)}(r_>,E_7)]\,r_1f_{6p}(r_1)\,dr_1\,dr_2}{J(E_7)}\Big]$$
$$-\tfrac{2}{9}\times(\text{same as above with }\kappa=+2). \tag{C9}$$

In all of the above expressions, $r_>=\max(r_1,r_2)$ and $r_<=\min(r_1,r_2)$. The expression for β [Eq. (83)] is obtained in the same way.

---

*Research supported by United States Energy Research and Development Administration.

[1]F. J. Hasert *et al.*, Phys. Lett. 46B, 121, 138 (1973); Nucl. Phys. B 73, 1 (1974); A. Benvenuti *et al.*, Phys. Rev. Lett. 32, 800 (1974); 37, 1039 (1976); B. Aubert *et al.*, Phys. Rev. Lett. 32, 1454 (1974); S. J. Barish *et al.*, Phys. Rev. Lett. 33, 418 (1974); 36, 179 (1976); B. C. Barish *et al.*, Phys. Rev. Lett. 34, 538 (1975); W. Lee *et al.*, Phys. Rev. Lett. 37, 186 (1976); see C. H.Albright *et al.*, FERMILAB-Pub.-76/40-Thy (unpublished), report of a recent review of the high-energy experimental situation.

[2]S. Weinberg, Phys. Rev. Lett. 19, 1264 (1967); 27, 1688 (1971); Phys. Rev. D 5, 1412 (1972); A. Salam, in *Elementary Particle Theory*, edited by N. Svartholm (Almquist and Forlag, Stockholm, 1968); for a review of renormalizable gauge theories, see T. D. Lee, Phys. Rep. 9C, No. 2 (1974) and J. C.Taylor, *Gauge Theories of Weak Interactions* (Cambridge University. London, 1976).

[3]S. Chu, E. D. Commins, and R. Conti, Phys. Lett. 60A, 96 (1977); S. Chu, Ph.D. thesis, Lawrence Berkeley Laboratory report LBL-5731 (unpublished).

[4]M. A. Bouchiat and C. C. Bouchiat, Phys. Lett. 48B, 111 (1974); J. Phys. (Paris) 35, 899 (1974); 36, 493 (1975).

[5]T. Tietz, J. Chem. Phys. 22, 2094 (1954).

[6]M. E. Rose, *Relativistic Electron Theory* (Wiley, New York, 1961). Our f and g are not the same as Rose's.

[7]C. Schwartz, Phys. Rev. 97, 380 (1955); 105, 173 (1957).

[8]M. Abramowitz and I. A. Stegun, *Handbook of Mathematical Functions*, NBS Appl. Math. Ser. 55 (U.S. GPO, Washington, D. C., 1964).

[9]C. M. Lederer, J. M. Hollander, and I. Perlman, *Table of Isotopes* (Wiley, New York, 1967).

[10]V. B. Berestetskii, E. M. Lifschitz, and L. P. Pitaevskii, *Relativistic Quantum Theory*, Vol. 4, Pt. I of *Course of Theoretical Physics* (Pergamon, London, 1971).

[11]A. Gallagher and A. Lurio, Phys. Rev. 136, A87 (1964).

[12]E. M. Anderson, E. K. Anderson, and V. F. Trusov, Opt. Spektrosk. 22, 861 (1967) [Opt. Spectrosc. (USSR) 22, 471 (1967)].

[13]W. R. Johnson, Phys. Rev. Lett. 29, 1123 (1972).

[14]M. Phillips. Phys. Rev. 88, 209 (1952).

[15]G. Breit, Phys. Rev. 34, 553 (1929); 39, 616 (1932).

[16]A. Abragam and J. H. Van Vleck, Phys. Rev. 92, 1448 (1953).

[17]C. Schwartz (unpublished).

[18]W. E. Lamb, Jr., Phys. Rev. 60, 817 (1941).

[19]T. R. Fowler, Ph.D. thesis (UCRL-18321) (University of California, 1968) (unpublished).

[20]R. H. Garstang, J. Res. Natl. Bur. Stand. (U.S.) A 68,

61 (1964).
[21]F. Reines *et al.*, Phys. Rev. Lett. 37, 315 (1976).
[22]O. P. Sushkov, V. V. Flambaum, and I. B. Khriplovich, Zh. Eksp. Teor. Fiz. Pis'ma Red. (to be published) [JETP Lett. 24, 502 (1976)].
[23]E. M. Henley and L. Wilets, Phys. Rev. A 14, 1411 (1976).
[24]M. Brimicombe, C. E. Loving, and P. G. H. Sanders, J. Phys. B 9, L237 (1976).
[25]E. Fermi and E. Segre, Z. Phys. 82, 729 (1933).
[26]G. F. Koster, Phys. Rev. 96, 148 (1952).
[27]P. J. Mohr, Ann. Phys. (N.Y.) 88, 26 (1974).
[28]M. Gyulassy, Nucl. Phys. A 244, 497 (1975).
[29]This argument is originally due to Bouchiat and Bouchiat, Ref. 4.